The Journal of Immunology

High-Resolution Longitudinal Study of HIV-1 Env Vaccine–Elicited B Cell Responses to the Virus Primary Receptor Binding Site Reveals Affinity Maturation and Clonal Persistence

Yimeng Wang, Christopher Sundling, Richard Wilson, Sijy O'Dell, Yajing Chen, Kaifan Dai, Ganesh E. Phad, Jiang Zhu, Yongli Xiao, John R. Mascola, Gunilla B. Karlsson Hedestam, Richard T. Wyatt and Yuxing Li

J Immunol 2016; 196:3729-3743; Prepublished online 21 March 2016;
doi: 10.4049/jimmunol.1502543
http://www.jimmunol.org/content/196/9/3729

The Journal of Immunology is published twice each month by
The American Association of Immunologists, Inc.,
1451 Rockville Pike, Suite 650, Rockville, MD 20852

Print ISSN: 0022-1767 Online ISSN: 1550-6606.

High-Resolution Longitudinal Study of HIV-1 Env Vaccine–Elicited B Cell Responses to the Virus Primary Receptor Binding Site Reveals Affinity Maturation and Clonal Persistence

Yimeng Wang,[*,†] Christopher Sundling,[‡,§] Richard Wilson,[¶] Sijy O'Dell,[‖] Yajing Chen,[*] Kaifan Dai,[*] Ganesh E. Phad,[‡] Jiang Zhu,[*,#] Yongli Xiao,[**] John R. Mascola,[‖] Gunilla B. Karlsson Hedestam,[‡] Richard T. Wyatt,[*,¶,#] and Yuxing Li[*,†,¶]

Because of the genetic variability of the HIV-1 envelope glycoproteins (Env), the elicitation of neutralizing Abs to conserved neutralization determinants including the primary receptor binding site, CD4 binding site (CD4bs), is a major focus of vaccine development. To gain insight into the evolution of Env-elicited Ab responses, we used single B cell analysis to interrogate the memory B cell Ig repertoires from two rhesus macaques after five serial immunizations with Env/adjuvant. We observed that the CD4bs-specific repertoire displayed unique features in the third CDR of Ig H chains with minor alterations along the immunization course. Progressive affinity maturation occurred as evidenced by elevated levels of somatic hypermutation (SHM) in Ab sequences isolated at the late immunization time point compared with the early time point. Abs with higher SHM were associated with increased binding affinity and virus neutralization capacity. Moreover, a notable portion of the CD4bs-specific repertoire was maintained between early and late immunization time points, suggesting that persistent clonal lineages were induced by Env vaccination. Furthermore, we found that the predominant persistent CD4bs-specific clonal lineages had larger population sizes and higher affinities than that from the rest of the repertoires, underscoring the critical role of Ag affinity selection in Ab maturation and clonal expansion. Genetic and functional analyses revealed that the accumulation of SHM in both framework regions and CDRs contributed to the clonal affinity and antigenicity evolution. Our longitudinal study provides high-resolution understanding of the dynamically evolving CD4bs-specific B cell response after Env immunization in primates. ***The Journal of Immunology*****, 2016, 196: 3729–3743.**

A successful HIV-1 vaccine is expected to elicit both T cell–mediated immunity and protective long-lasting Ab responses mediated by B cells (1). However, elicitation of potent and broadly neutralizing Ab (bNAb) response against circulating HIV-1 strains has been a major challenge. So far, all mAbs that display broadly neutralizing activity are isolated from chronically HIV-1–infected individuals. These bNAbs bind to conserved epitopes on the HIV-1 envelope glycoprotein (Env), which consists of the exterior gp120 and the transmembrane gp41 envelope proteins. Various conserved epitopes on Env are targeted by bNAbs, such as the membrane proximal external region of gp41 targeted by 2F5, 4E10, and 10E8, glycan-containing epitopes associated with V2 by PG9/PG16 and V3 by PGT121/PGT135/PGT128, the CD4 binding site (CD4bs) by VRC01, b12, and others, and quaternary epitopes overlapping gp120 and gp41 by PGT151, 35O22, and 8ANC195 (reviewed by Refs. 2–4). bNAbs

*Department of Immunology and Microbial Science, The Scripps Research Institute, La Jolla, CA 92037; [†]Institute for Bioscience and Biotechnology Research, University of Maryland, Rockville, MD 20850; [‡]Department of Microbiology, Tumor and Cell Biology, Karolinska Institutet, SE-171 77 Stockholm, Sweden; [§]Immunology Division, Garvan Institute of Medical Research, Darlinghurst, New South Wales 2010, Australia; [¶]International AIDS Vaccine Initiative Neutralizing Antibody Center at The Scripps Research Institute, La Jolla, CA 92037; [‖]Vaccine Research Center, National Institute of Allergy and Infectious Diseases, National Institutes of Health, Bethesda, MD 20892; [#]Scripps Center for HIV Vaccine Immunogen Discovery, La Jolla, CA 92037; and **Laboratory of Infectious Diseases, National Institute of Allergy and Infectious Diseases, National Institutes of Health, Bethesda, MD 20892

ORCIDs: 0000-0002-6138-690X (C.S.); 0000-0002-7718-5344 (R.W.); 0000-0001-8330-3901 (Y.C.); 0000-0002-0047-6899 (G.E.P.).

Received for publication December 8, 2015. Accepted for publication March 1, 2016.

This work was supported by National Institutes of Health, National Institute of Allergy and Infectious Diseases Grants R01 AI102766 (to Y.L.), P01 AI104722 (to R.T.W., Y.L., and G.B.K.H.), and UM1 AI100663 (to R.T.W. and J.Z.); Karolinska Institutet funds and foundations (to C.S.); the Swedish Physicians against AIDS Research Foundation (to C.S.); a Swedish Research Council International Postdoctoral Fellowship (to C.S.); the Swedish Research Council (to G.B.K.H.); the Intramural Research Program of the Vaccine Research Center, the National Institute of Allergy and Infectious Diseases, and the National Institutes of Health (to J.R.M.); and the International AIDS Vaccine Initiative (to R.T.W.) with generous support from the U.S. Agency for International Development, the Ministry of Foreign Affairs of the Netherlands, and the Bill & Melinda Gates Foundation (a full list of International AIDS Vaccine Initiative donors is available at http://www.iavi.org).

The sequences presented in this article have been submitted to GenBank (http://www.ncbi.nlm.nih.gov/genbank/) under accession numbers KU750814–KU751671 and KU761300.

The contents of this manuscript are the responsibility of the authors and do not necessarily reflect the views of the U.S. Agency for International Development or the U.S. Government.

Address correspondence and reprint requests to Dr. Yuxing Li, Institute for Bioscience and Biotechnology Research, University of Maryland, 9600 Gudelsky Drive, Rockville, MD 20850. E-mail address: yuxingli@umd.edu

The online version of this article contains supplemental material.

Abbreviations used in this article: BLI, biolayer light interferometry; bNAb, broadly neutralizing Ab; CD4bs, CD4 binding site; CDR3, third CDR; CDRH3, H chain CDR3; DSC, differential scanning calorimetry; Env, envelope glycoprotein; FR, framework region; Geomean, geometric mean; GRAVY, grand average hydropathy; Imm 2, second immunization; NGS, next-generation sequencing; NHP, nonhuman primate; Pst^{hi}, high persistence; Pst^{lo}, low persistence; RT, reverse transcription; SHM, somatic hypermutation; T_m, melting temperature; WT, wild type.

in general display unique features such as high degree of somatic hypermutations (SHMs), long length of the third CDR of Ig H chain, and restricted Ig germline usages (2–4). Among these epitopes, the CD4bs is an ideal target for a bNAb-eliciting vaccine because it is a highly conserved functional element, engaging Env to bind its primary receptor, CD4.

To efficiently elicit CD4bs-specific bNAb response in a vaccine setting, current effort in the field is focused on designing immunogens that closely mimic the antigenicity of the native Env functional trimer spike (5–7), robustly activate the bNAb germline precursors, especially CD4bs-specific Ab germlines (8–10), using Env variants isolated from natural infection at time points associated with the broadening of serum neutralization activities (11), or Env trimer cocktails to elicit cross-reactive neutralizing Ab responses (12). In parallel with the development of the next generation of vaccine candidates with the improved potential to elicit CD4bs-specific neutralizing Abs, it is crucial to understand how HIV-1 vaccine–elicited CD4bs-specific Ab responses dynamically evolve throughout immunization.

Several HIV-1 vaccine efficacy trials in humans have been performed, with only the RV144 trial displaying a modest protection efficacy (13). In one study, Ab response targeting HIV-1 gp120 major variable regions, V1/V2, was found to correlate with protection (14). Vaccine efficacy in this trial was not durable, peaking at ∼60.5% and then waning to background in 3 y, thus resulting in an average efficacy of 31.2% (15). This transient protection may be due to the fact that the protective Ab responses elicited by the vaccine are not persistent (16). However, it is not clear whether HIV-1 vaccines generally induce only transient B cell responses. Therefore, investigating the persistence of Ab responses is critical, and a comprehensive longitudinal analysis of the genetics, functionality, and durability of Ab responses induced by HIV-1 Env immunization should be conducted, as done in this study.

Nonhuman primate (NHP) models offer unique opportunities for HIV-1 vaccine studies, because of the similarity in the genetics and physiology between macaques and humans, as well as their susceptibility to infection with simian immunodeficiency viruses and chimeric simian HIV. The technologies to isolate Ag/epitope-specific NHP B cells followed by single-cell RT-PCR amplification, recombinant mAbs expression, and next-generation sequencing (NGS) technology can be successfully applied to analyze Env Ab responses in vivo at high resolution (17–19). However, it is not well-known how the Env- or CD4bs-specific memory B cell response is initially elicited and how it evolves during the immunization course, as well as how this process leads to the Ab affinity maturation and virus neutralization.

In this study, we integrated these technologies to characterize and delineate the evolution of CD4bs-specific clonal lineages during serial immunizations of NHPs. We found that compared with the highly diversified Env-specific Ab response, the CD4bs-specific Ab response had lower diversity with unique genetic and functional properties. A notable fraction of the Env- and CD4bs-specific memory B cell lineages was maintained and persisted during the course of the immunization regimen. Primarily driven by Ag affinity selection, these progressively accumulated SHMs led to elevated Env-binding affinity and expanded virus neutralization capacity. Investigation of persistent and predominant CD4bs-specific clonal lineages revealed that affinity maturation attributed to SHM occurred in both framework regions (FRs) and CDR regions, which led to substantial change of the Ab molecule thermostability and partial footprint shifts on the gp120 surface. The high-resolution longitudinal analysis of Ab clonal lineages targeting the HIV-1 primary receptor binding site epitope presented in this study provides insight into the evolution of B cell responses after HIV-1 Env immunization, expanding information important for vaccine development.

Materials and Methods

Samples for B cell repertoire data collection

Rhesus macaques were immunized five times on a monthly interval with recombinant YU2 gp140-F trimer/AbISCO and CpG adjuvant. Peripheral blood was collected 1–3 wk after each immunization, followed by PBMC preparation as described previously (20). In this study, frozen PBMCs from Rhesus macaques F125 and F128 at 1–3 wk after the second immunization (Imm 2) and Imm 5 were used.

Cell staining and single-cell flow cytometric sorting

PBMCs were stained as described previously (18). In brief, frozen PBMCs were thawed and treated with 10,000 U/ml DNase I (Roche) in RPMI 1640 supplemented with 10% FBS media, followed by Aqua Dead Cell Staining (Life Technologies). A mixture of Abs containing CD3 (allophycocyanin-Cy7; SP34-2; BD Pharmingen), CD8 (Pacific blue; RPA-T8; BD Pharmingen), CD14 (Qdot 605; M5E2, VRC), CD20 (PE-Alexa Fluor 700; 2H7, VRC), CD27 (PE-Cy7; M-T271; BD Pharmingen), IgG (FITC; G18-145; BD Pharmingen), and IgM (PE-Cy5; G20-12; BD Pharmingen) was used to stain the PBMCs. To sort Env and CD4bs-specific B cells, we incorporated gp140-F conjugated with streptavidin-allophycocyanin conjugate (Life Technologies) and gp140-F-D368R with streptavidin-PE conjugate (Life Technologies) in the earlier stated Ab mixture. After staining, the cells were sorted at a single-cell density into 96-well plates with lysis buffer using a four-laser FACSAria III cell sorter. Env-specific memory B cells were defined as $CD3^-CD8^-$Aqua $Blue^-CD14^-CD20^+IgG^+CD27^+IgM^-$gp140-$F^{hi}$, whereas CD4bs-specific memory B cells were defined as $CD3^-CD8^-$Aqua $Blue^-CD14^-CD20^+IgG^+CD27^+IgM^-$gp140-$F^{hi}$gp140-F–$D368R^{lo}$.

Single-cell RT-PCR

The sorted cells were lysed by the lysis buffer followed by single-cell reverse transcription (RT) and PCRs to amplify Ig sequences as described previously (21, 22). In brief, in each well containing lysed cell, 150 ng random hexamers, 0.4 mM dNTPs, 100 U SuperScript III (Life Technologies), and 3.5 μl water were added, followed by incubation at 42˚C for 10 min, 25˚C for 10 min, 50˚C for 60 min, and 94˚C for 5 min to generate cDNA. Nested PCR was then performed with 2 μl cDNA in 25-μl reactions with the HotStar Taq Plus Kit (QIAGEN), using 5′ leader sequence–specific and 3′ IgG-specific primers (22). In the second round of nested PCRs, 1.75 μl of the first PCR product was used as a template. All nested PCRs were incubated at 94˚C for 5 min followed by 50 cycles of 94˚C for 30 s, 50˚C (H chain) or 52˚C (κ- or λ-chain) for 45 s, and 70˚C for 1 min with a final elongation at 70˚C for 10 min before cooling to 4˚C. Nested PCR products were evaluated on 2% 96-well E Gel (Life Technologies), and positive wells with a specific band of ∼450 bp were purified and sequenced.

Ab cloning

A cloning PCR was performed in a total volume of 50 μl with 1 μl of the second nested PCR product as template, using Expand High-Fidelity PCR Kit according to the manufacturer's instructions (Roche). In brief, the PCR consisted of 5 μl of 10× reaction buffer, 1 μl 10 mM dNTPs, 1 μl each of 25 μM of 3′ and 5′ cloning primers, 1 μl DNA polymerase, and water to 50 μl. The cloning primers were described previously (22). The PCR had an initial denaturation at 95˚C for 3 min, followed by 20 cycles of 95˚C for 30 s, 50˚C for 30 s, and 68˚C for 2 min. There was a final elongation at 68˚C for 8 min before cooling to 4˚C followed by evaluation on 1% agarose gel. Positive bands (∼400 bp for H chain VDJ and ∼350 bp for L chain VJ] were then purified, digested with restriction enzymes, and ligated into eukaryotic expression vectors containing human Igγ1H, Igγ2, or Igκ1 L chain Ab expression cassettes (23, 24). After transformation of ligated products into competent cells, bacterial colonies were sequenced for insertion of correct sequences.

Ab expression and specificity binding test

The Ab H and L chain expression vectors carrying the correct insertions were transfected at an equal ratio into 293F cells, cultured at an initial density of 1 million cells per milliliter, using 293fectin Transfection Reagent (Life Technologies) as described previously (22). Four days after the transfection, the cell culture supernatants were harvested and purified

by protein A-Sepharose columns packed in-house (GE Healthcare). The purified Abs were further tested for specificity by ELISA.

MaxiSorp plates (Nunc, Thermo Scientific) were coated with 0.2 μg Ag gp140-F or mutant gp140-F-D368R (CD4bs binding knockout) in 100 μl PBS per well overnight at 4°C. After the plates were washed with PBS/0.2% Tween 20 and blocked with PBS/2% dry milk/5% FBS for 1 h at 37°C, purified Abs were added into wells in 5-fold dilution series, starting from 10 μg/ml, and incubated for 1 h at 37°C. HRP-conjugated goat-human IgG (Jackson Immunoresearch) was then used at a 1:10,000 dilution in PBS/0.2% Tween 20 and incubated for 1 h at room temperature. The bound Ab was detected with 100 μl/well TMB substrate (Life Technologies) for 5 min before the reaction was stopped by addition of 100 μl 3% H_2SO_4. The OD was measured at 450 nm. Between each step of the ELISA, plates were washed four times with PBS supplemented with 0.2% Tween 20.

Single-cell–sorted B cell Ig sequence genetic analysis

The single-cell RT-PCR–generated Ab V(D)J gene segments were analyzed by two approaches. For overall H chain VDJ family analysis, sequences were initially analyzed by IMGT/High V-Quest (25) (version 1.1.3, reference directory release 201338-1; http://imgt.cines.fr) to define Ig subdomains. For a more exhaustive annotation of the individual H and L chain V(D)J gene segments, Ab sequences were processed through IgBLAST version 1.1.0 (26) using previously published rhesus macaque germline databases (18, 22), as well as IGD and IGJ databases from IMGT to deduce gene segment usage. SHM was evaluated at the nucleotide level by alignment of single-cell–sorted sequences against the corresponding assigned germline sequences using IgBLAST version 1.1.0 (26). When SHM at the level of amino acid was calculated, nucleotide sequences in rhesus macaque germline databases were translated into peptide sequences to form germline peptide sequence database. The query nucleotide sequences (single-cell–sorted sequences) were also subsequently translated and aligned to its corresponding identified sequence in rhesus macaque germline peptide databases by blastx in blast-2.2.26+ package (27) to evaluate SHM. Clonal lineages are defined by the usage of V and J segments, third CDR (CDR3) length, and CDR3 homology (>90%). CDR3 was defined using IMGT/High V-Quest, as stated later. The Ig molecule encoding sequences generated from single B cell sorting and RT-PCR amplification are available with accession numbers KU750814–KU751671 and KU761300 at GenBank (http://www.ncbi.nlm.nih.gov/genbank/). The sequences are being reported on in this article for the first time. Sequences with GenBank accession numbers KF947536-KF948098 (Env-specific), KF948099-KF948514 (Total), and JQ885990-JQ886005 (CD4bs) generated from previous studies (17, 18) were also included in the analysis.

CDR3 analysis

CDR3 amino acid sequences, including the conserved 5′ cysteine (C) and 3′ tryptophan (W) residues, were obtained by querying Ab nucleotide sequences with IMGT/High V-Quest function using the rhesus macaque and human germline databases. The contribution of each amino acid to the individual CDR3 was then determined. CDR3 hydrophobicity was investigated by calculating the grand average hydropathy (GRAVY) score, using the online calculator provided by Dr. Stephan Fuchs (http://www.gravy-calculator.de). The GRAVY score is defined by the sum of hydrophobicity of all amino acids divided by the peptide length, with a higher score indicating a higher hydrophobicity of the peptide.

Bioinformatics analysis of Ab NGS data

Single-cell RT-PCR–amplified sequences, as template sequences, were querying against the NGS database obtained from animal F128 Imm 5 [17] to identify somatic variants and to generate identity/divergence plots. The NHP Ab NGS data were processed and analyzed using a bioinformatics pipeline developed based on the framework of a human antibodyomics pipeline (28). Given a data set of NGS-derived NHP Ab sequences, each sequence was: 1) reformatted and labeled with a unique index number; 2) assigned to V, D (for H chain only), and J gene families using the rhesus macaque germline gene database (18, 22) and an in-house implementation of IgBLAST, with sequences possessing an E value $>10^{-3}$ for V gene assignment removed from the data set; 3) subjected to a template-based, error-correction procedure, in which insertion and deletion (indel) errors of less than three nucleotides in the V gene segment were detected by alignment to their respective germline gene sequences and subsequently corrected; 4) compared with the template Ab sequences at both nucleotide level and amino acid level using a global alignment module in CLUSTALW2 (29), which provides the basis for identity/divergence analysis (e.g., Supplemental Fig. 2); and 5) subjected to a multiple sequence alignment–based procedure to determine CDR3, which was further compared with the template CDR3 sequences at the nucleotide level, and to determine the sequence boundary of the V(D)J coding region. After full-length V region sequences were obtained, a bioinformatics filter was applied to detect and remove erroneous sequences that may contain swapped gene segments because of PCR errors. Specifically, a full-length read would be removed if the V-gene alignment was <250 bp.

Ab binding affinity

Biolayer light interferometry (BLI) was performed using an Octet RED96 instrument (ForteBio; Pall Life Sciences). The purified Abs were captured onto anti-human IgG Fc biosensors and monomeric YU2gp120, purified by affinity chromatograph followed by size-exclusive chromatography, was diluted in 2-fold series starting from 250 to 7.8 nM as the analyte in solution. The biosensors were hydrated for 10 min in PBS with 0.2% Tween 20 as the binding buffer. In brief, the biosensors were first immersed in binding buffer for 60 s to establish a baseline and then in a solution containing 10 μg/ml NHP or human Env-specific mAbs for 60 s to capture the mAb. The biosensors were then submerged in binding buffer for a wash of 60 s. The biosensors were then immersed in a solution containing various concentrations of gp120 for 120 s for analyte–ligand association, followed by 120 s in binding buffer to assess analyte–ligand dissociation. Binding affinity constants (dissociation constant, K_D; on-rate, k_{on}; off-rate, k_{off}) were determined using Octet Analysis version 7 software.

HIV-1 neutralization assays

Ab neutralization assays were performed with the format of single round of infection using HIV-1 Env-pseudoviruses and TZM-bl target cells, as described previously (30–32). Neutralization curves were fit by nonlinear regression using a five-parameter hill slope equation as previously described (31). The IC_{50} of Ab were reported as the concentration of Ab required to inhibit infection by 50%. The IC_{50} geometric mean (Geomean) indicating mAb neutralization potency was derived from IC_{50} values against each individual tier 1 virus for each mAb. When IC_{50} value is >50 μg/ml for certain viruses (no neutralization), a value of 50 μg/ml is designated for calculation. The number of viruses neutralized by mAb (IC_{50} < 50 μg/ml) out of the total number of tested tier 1 viruses was used to calculate the neutralization breadth.

GEAT361 lineage germline precursor inference

Germline V(D)J genes were assigned using previously published custom databases (18, 22) in IgBLAST (PMID 23671333). Assigned V(D)J germline genes were aligned to the query sequence and manually inspected to determine junctional diversity caused by the trimming P and N nucleotides. In the germline reverted clones, the junctions were retained whereas the V(D)J genes were reverted to germline nucleotide sequence.

Differential scanning calorimetry

Differential scanning calorimetry (DSC) experiments were performed using N-DSC II differential scanning calorimeter (Calorimetry Sciences). Ab samples, purified by protein A column followed by size-exclusive chromatography to remove aggregates and dimers, at concentration of 0.57 mg/ml in PBS were scanned at rate of 1 K/min under 3.0 atm of pressure. DSC data were analyzed using NanoAnalyze software (TA Instruments).

Ala scanning and molecular modeling

A panel of 27 JRCSF gp120 Ala mutants containing alterations known to affect sCD4 or a set of known CD4bs-specific mAb binding (18, 22) was selected. The Ala mutations were generated previously (33) in the context of the full-length JRCSF gp160. The gp120 was released from the pseudoviruses by detergent lysis and captured by the sheep anti-gp120 C5 Ab, D7324 (Aalto Bio Reagents), previously coated on ELISA plates. After washing, Ab binding affinity to gp120 variants was assessed as described later. The level of binding by the human mAb 2G12 and was used to normalize the variant gp120 expression levels. The effect of a given Ala mutation on Ab binding was represented by apparent affinity (avidity) relative to the binding level to the wild type (WT) gp120, calculated with the formula of ((EC_{50}_WT/EC_{50}_mutant)/[EC_{50}_WT for 2G12 (or HIVIg)/EC_{50}_mutant for 2G12 (or HIVIg)]) × 100, where EC_{50} is the median effective concentration as previously described (33). Based on alanine mapping results, we highlighted the binding specificities of representative NHP Imm 2 and Imm 5 mAbs by using the gp120 core crystal structure PDB-2NY3 from Protein Data Bank (34).

Statistical analysis

The comparison of V(D)J-family distributions between the Env- and CD4bs-specific Ig repertoires was analyzed with the χ^2 test. Comparisons of individual V-gene segment contributions to the Env- and CD4bs-specific Ig repertoires were carried out with two-way ANOVA. Evaluation of three or more groups was done with one-way ANOVA. Unless mentioned otherwise, statistical evaluation between two groups was performed with *t* test or Mann–Whitney test. The correlation was determined with the nonparametric Spearman correlation test, with a two-tailed *p* value calculated for significance. Statistical significance was determined as $*p < 0.05$, $**p < 0.01$, $***p < 0.001$, $****p < 0.0001$. All statistical analysis was performed with GraphPad Prism version 6.

Results

HIV vaccine–elicited Ig repertories from rhesus macaques immunized with trimeric YU2 gp140F

Chinese rhesus macaques, designated as F125 and F128, were immunized monthly with well-characterized first generation of trimeric HIV-1 Env YU2 gp140-F in adjuvant as previously described (20). Vaccine-elicited Env- and CD4bs-specific memory B cells were sorted from PBMCs 1–3 wk after Imm 2 and Imm 5, respectively, using FACS-based multicolor epitope-specific single B cell sorting technology developed previously (Fig. 1A) (17). Env- and CD4bs-specific memory B cells were gated as $CD20^+IgG^+IgM^-CD27^+$gp140-F^{hi} and $CD20^+IgG^+IgM^-CD27^+$gp140-F^{hi}/gp140-F–D368R^{lo}, respectively (Fig. 1A). We observed that Env- and CD4bs-specific memory B cells accounted for ∼5 and 0.2% of total memory B cells, respectively (Fig. 1A), consistent with the results of our previous studies (18). After cell lysis, RT of the mRNA and nested PCR were conducted to recover the variable regions of Ig H/L chains. After sequence verification and phylogenetic analysis, we characterized the genetic composition of the Env- and CD4bs-specific Ig repertories.

The sorting specificity was confirmed by cloning selected amplicons into Ig H/L chain expression vectors (22–24) to produce a panel of NHP mAbs for Env-binding and virus neutralization assays. The criteria for selecting amplicons for cloning and expression were that the sequences should represent the genetic diversity of the amplicons by phylogenetic analysis and have matched H and L chain amplicons available after PCR amplification. A total of 34 mAb clones, accounting for >10% of the total amplified 292 CD4bs-specific H chain Ig clones, were selected for expression and characterization. The binding specificity

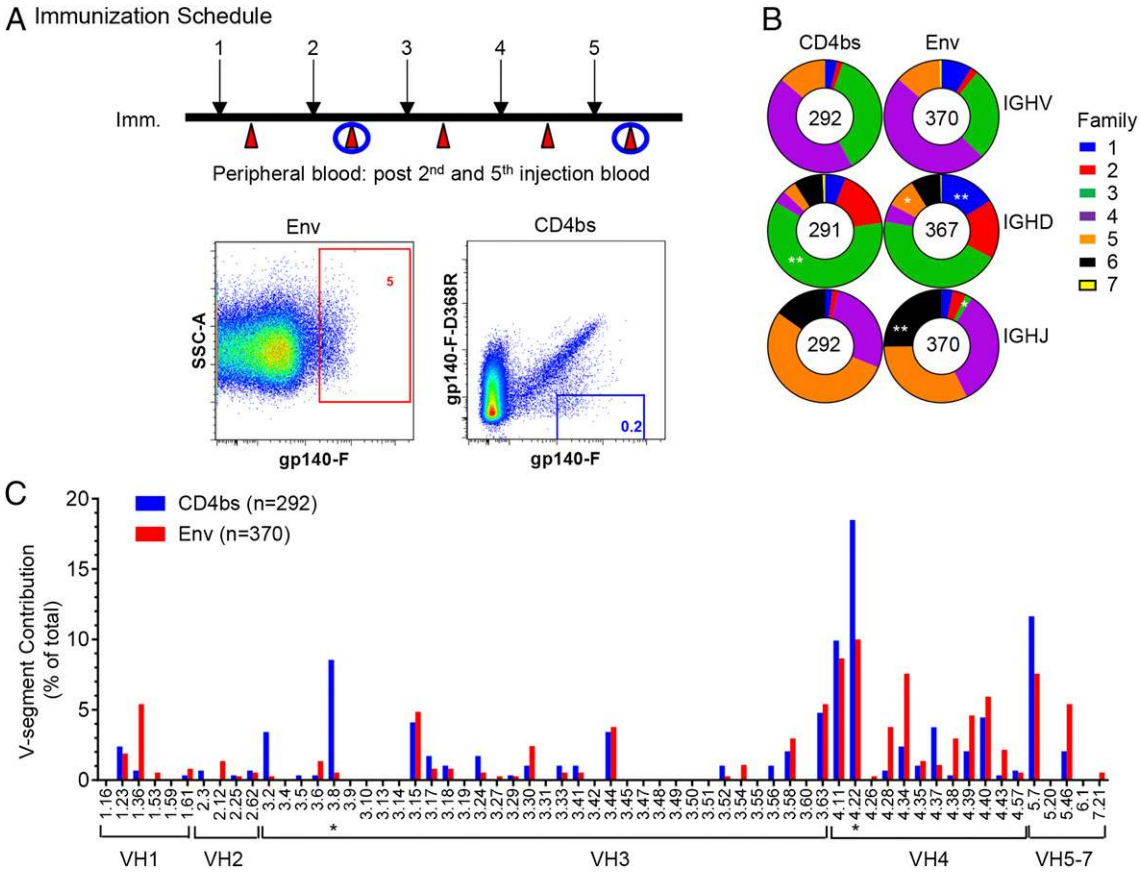

FIGURE 1. Isolation of vaccine-induced NHP Ag-specific single-cell and Ag-specific IgH gene segment usage. (**A**) Schematic presentation of the immunization schedule and Ag-specific B cell sorting. *Upper panel*, Immunization/sampling schedule. Whole blood samples from two macaques inoculated with HIV Env YU2gp140-F trimer five times in a monthly interval (black arrow) were collected 1–3 wk after each inoculation (red arrow) to prepare PBMCs (20). PBMCs from time points after the Imm 2 and Imm 5 were subjected to single-cell sorting, indicated with blue circles. *Lower panel*, Single-cell sorting for Env- and CD4bs-specific memory B cells. IgG memory B cells were defined as $CD3^-/CD8^-$/Aqua $Blue^-/CD14^-/CD20^+/IgG^+/CD27^+/IgM^-$. Env- and CD4bs-specific memory B cells were then gated by phenotype of gp140-F^{hi} and gp140-F^{hi}/gp140-F–D368R^{lo}, respectively. Gate frequency (percent) of Env- and CD4bs-specific memory B cells out of total memory B cells is depicted in red and blue, respectively. (**B**) IGHV-, D-, and J-family Ig-gene usage of sorted Env- and CD4bs-specific memory B cells, defined by IgBLAST and IMGT/High V-Quest. H chain gene families are color coded, with size of the colored area corresponding to the frequency (percent) out of the total number of sequences indicated in the center of the graphs. Differences in the gene family usage between the Env- and CD4bs-specific Ig repertoires were evaluated using χ^2 test. $*p < 0.05$, $**p < 0.01$. (**C**) Env- (red) and CD4bs (blue)-specific Ig repertoire V-gene segment contribution to the total number of sequences of each individual repertoire. VH3.8 and VH4.22, overexpressed in CD4bs-specific Ig repertoire, were marked with an asterisk. Two-way ANOVA was used for statistical analysis. $*p < 0.05$.

of the sorted CD4bs-specific mAbs was confirmed by binding affinity to trimeric YU2gp140-F and the CD4bs-knockout mutant, YU2gp140-F-D368R via ELISA assays. Among the 34 cloned putative CD4bs-specific mAbs, all 34 (100%) bound gp140-F, and 30 (88%) displayed the expected gp140-F^{hi}/gp140-F-D368R^{lo} binding phenotype (data not shown), which is consistent with the sorting precision in previous studies (18). Taken together, the Ag binding specificity of the single-cell–sorted Ig repertoires is validated, enabling further genetic analysis of the Env- and CD4bs-specific Ab repertoire along the immunization course.

Genetic characterization of HIV vaccine–elicited Env- and CD4bs-specific Ig repertoires

To investigate the genetic composition of the HIV vaccine–elicited Env- and CD4bs-specific Ig repertoires, we analyzed the single-

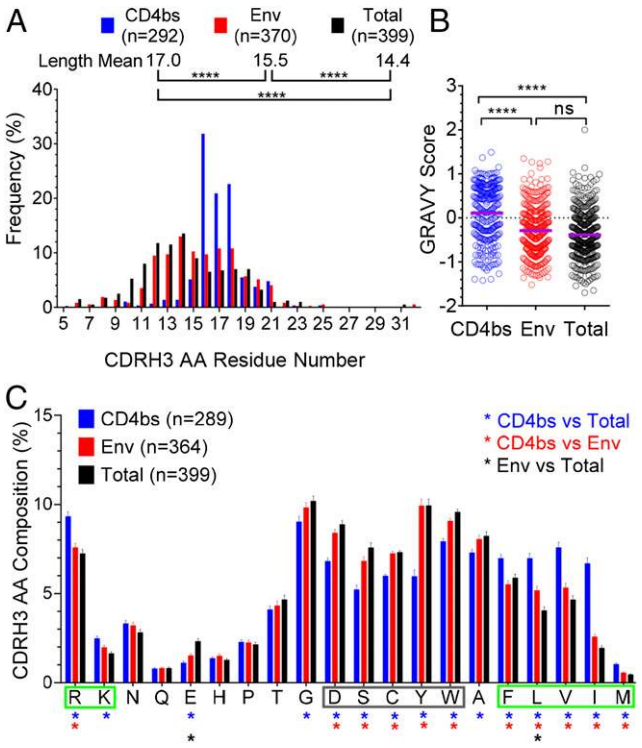

FIGURE 2. The unique genetic and functional features of CD4bs-specific Ig repertoire CDRH3 region. (**A**) The comparison of CDRH3 amino acid length of single-cell–sorted CD4bs- (blue), Env-specific (red), and total (no Ag specificity) B cell (black) Ig sequences. CDRH3 region is defined based on the IMGT CDR3 definition. The individual CDRH3 length frequency out of the total number of CDRH3 region length was calculated and depicted. Statistical differences of CDRH3 length among CD4bs-, Env-specific, and total Ig compartments were evaluated using one-way ANOVA. The mean of amino acid length of each Ig repertoire is indicated. ****$p < 0.0001$. (**B**) The CDRH3 of CD4bs-specific Ig repertoire displayed hydrophobicity higher than that of the Env-specific and the total Ig repertoires indicated by GRAVY score. Statistical differences of CDRH3 GRAVY scores among the CD4bs-specific (blue), Env-specific (red), and total (black) Ig repertoires were evaluated using one-way ANOVA with ****$p < 0.0001$. (**C**) Comparison of amino acid residue contribution to CD4bs-specific, Env-specific, and total Ig CDRH3 regions. The contribution of each amino acid residue to individual CDRH3 was calculated and summarized for each Ig compartment. Statistical differences were evaluated using one-way ANOVA. Amino acid residues highlighted by a green box had an increased frequency in the CD4bs-specific compartment compared with the total compartment, whereas residues highlighted by a gray box had reduced frequency. Amino acid residues are displayed on the *x*-axis according to polarity, with charged residues to the *left* and hydrophobic residues to the *right*. *$p < 0.05$.

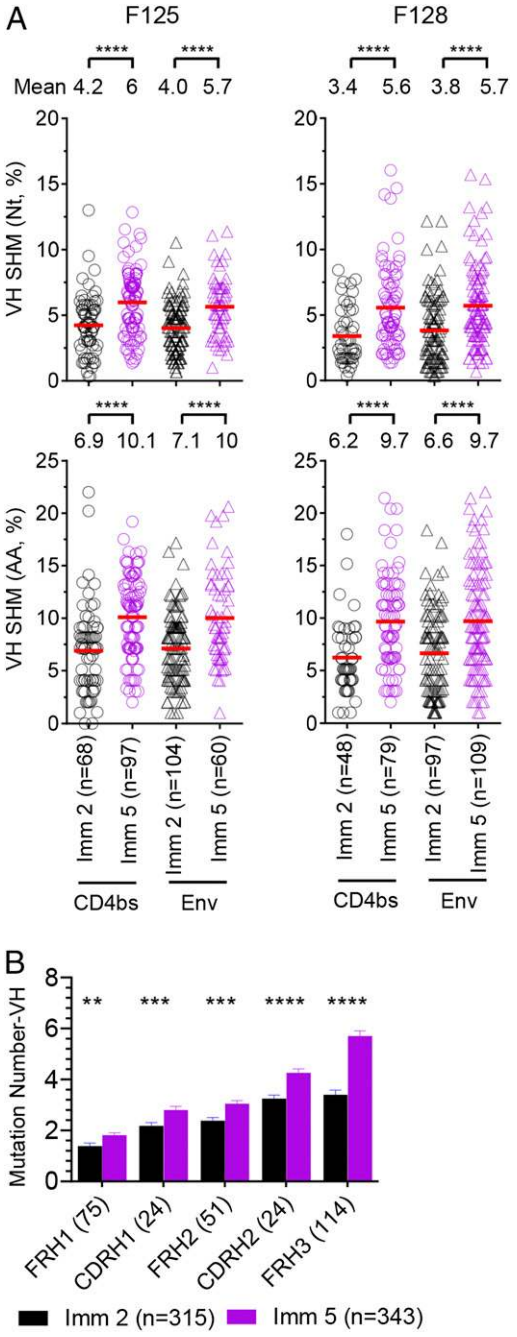

FIGURE 3. SHMs of the VH segments in CD4bs- and Env-specific Ig repertories indicate progressive affinity maturation during immunization. (**A**) VH SHM levels of single-cell–sorted Ag-specific Ig repertoires increase during the course of immunization from animals F125 (*left panels*) and F128 (*right panels*). H chain V-gene SHMs of single-cell–sorted Env (triangles) and CD4bs-specific (circles) repertoires at Imm 2 (black) and 5 (purple) are shown at nucleotide (Nt, *upper panels*) or amino acid (AA, *lower panels*) level. The mean of SHM percentage in each compartment is indicated. Statistical differences in SHM between Imm 2 and 5 were evaluated using one-way ANOVA. ****$p < 0.0001$. (**B**) Accumulated mutations within subdomains of VH region of all the VH amplicons from animals F125 and F128 during the course of immunization. Each Ab H chain VDJ sequence was divided into the subdomains of FRs and CDRs based on IMGT definition, with the number in parentheses indicating subdomain length. Each subdomain was further aligned to the corresponding germline to obtain nucleotide mutation number from Imm 2 (black) and 5 (purple) with VH sequences pooled from both animals. Statistical differences in mutation frequency were evaluated using the Mann–Whitney test. **$p < 0.01$, ***$p < 0.001$, ****$p < 0.0001$.

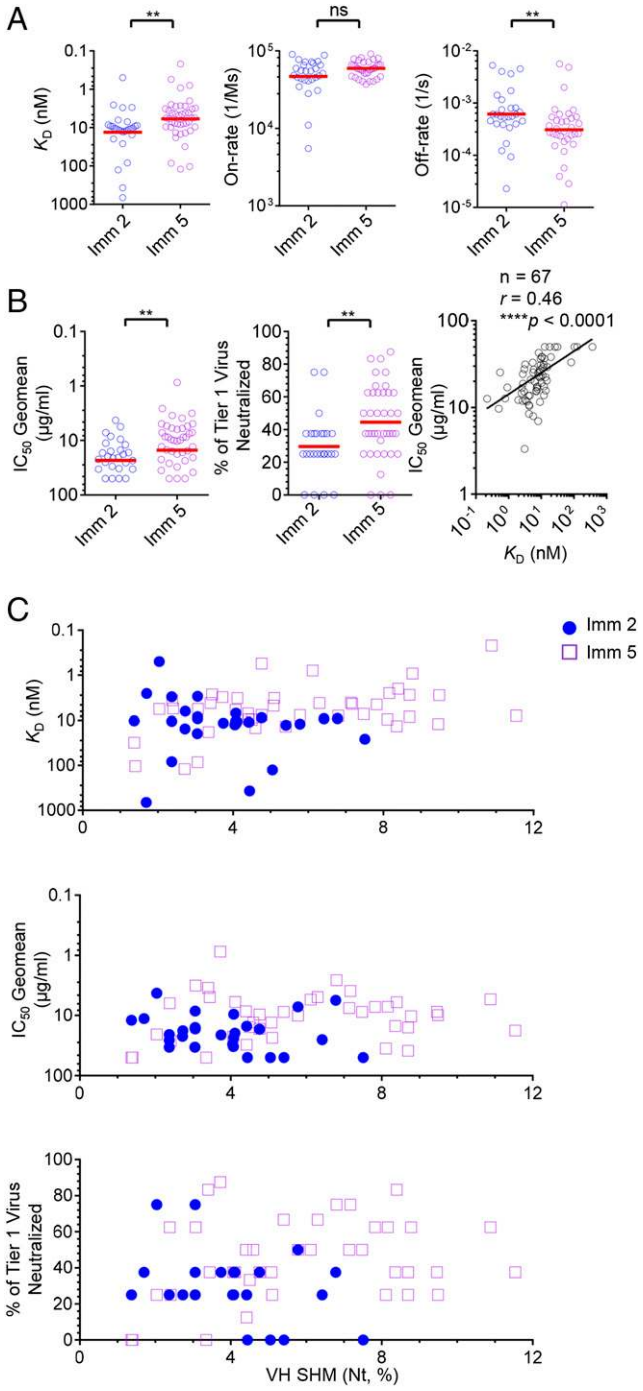

FIGURE 4. The functionality evolution of representative mAbs from CD4bs-specific Ig repertoire during the course of immunization. (**A**) Binding affinity of CD4bs-specific mAbs increased during the course of immunization. Representative mAbs were cloned from single-cell–sorted CD4bs-specific Ig sequences from Imm 2 and Imm 5 immunization time points with binding affinity to gp120 analyzed by BLI. The dissociation constants (K_D), association rates (on-rate), and dissociation rates (off-rate) of mAbs isolated from Imm 2 (blue) and 5 (purple) were compared using the Mann–Whitney test. $^{**}p < 0.01$. (**B**) The tier 1 virus neutralization capacity of CD4bs-specific mAbs increased during the course of immunization and was correlated with binding affinity. Eight tier 1 pseudoviruses were tested with the results reported as the neutralization IC_{50} value, the concentration of the mAb at which the virus entry is inhibited by 50%. The neutralization potency (*left panel*) and breadth (*middle panel*) were compared between mAbs from Imm 2 (blue) and Imm 5 (purple) and evaluated using the Mann–Whitney test. The correlation between binding affinity and neutralization potency was determined using the nonparametric Spearman test (*right panel*). Total mAb number (n), correlation coefficient (*r*), and the *p* value are shown. $^{**}p < 0.01$. (**C**) CD4bs-specific mAb repertoire possesses distinctive functionality and maturation properties at two different immunization time points. CD4bs-specific mAb VH nucleotide SHMs were plotted versus Ag binding affinity (K_D, *upper panel*), tier 1 virus neutralization potency (IC_{50} Geomean, *middle panel*), and neutralization breadth (% of tier 1 virus neutralized, *lower panel*) of time points Imm 2 (blue circles) and Imm 5 (purple hollow square), respectively.

cell–sorted sequences based on the rhesus monkey V(D)J database as described previously (18). In particular the germline gene segment usage was defined and the level of SHM, which represents the Ig sequence divergence from their germline ancestor and is critical for Ab affinity maturation, was evaluated. We found that both Env- and CD4bs-specific Ig repertoires had similar H chain gene family distributions, where most of the VH genes belong to germline VH3 and VH4 families, DH genes to DH3 family, and JH genes to JH4 and JH5 families (Fig. 1B), respectively. However, a significant overrepresentation of the DH3 family was noted in CD4bs-specific Ig repertoire compared with the Env-specific repertoire, whereas DH1, 5 and JH3, 6 families were significantly overrepresented in Env-specific Ig repertoire than CD4bs-specific repertoire ($^{*}p < 0.05$, $^{**}p < 0.01$, χ^2 test) (Fig. 1B). Upon closer examination of individual V-gene segment use of the H chain, VH3.8 and 4.22 were found to be used with significantly greater frequency in the CD4bs-specific repertoire than their usages in the Env-specific repertoire ($^{*}p < 0.05$, two-way ANOVA) (Fig. 1C).

In addition, the L (κ and λ) chains of both Env- and CD4bs-specific Ig repertoires also showed similar family distributions, where most of the VK genes belonged to the germline VK1 family, the VL genes to the VL2 family, the JK genes to the JK4 family, and the JL genes to the JL2 family (data not shown). Of note, there was significant overrepresentation of VL2 family use in the CD4bs-specific repertoire and VL3 use in the Env-specific repertoire ($^{*}p < 0.05$, χ^2 test) (data not shown). Upon closer examination of the individual V-gene segment use of L chains, VK2.51 was found to be more common in the Env-specific repertoire and VL2.7 more common in the CD4bs-specific repertoire ($^{*}p < 0.05$, two-way ANOVA) (data not shown), respectively.

In summary, although single-cell–sorted Env- and CD4bs-specific Ig repertoires possess overall similar germline gene segment profiles, significant biases do exist which might contribute to distinct biologic functions and relative degrees of clonal expansion.

H chain CDR3 sequences of the CD4bs-specific repertoire display unique features regarding length, hydrophobicity, and electrostatic properties

By sequence inspection, we observed several unique features of the CD4bs-specific Ig repertoire, which may be responsible for the distinct epitope recognition of these Abs, compared with the Env-specific and the total IgG repertoire. Examination of H chain CDR3 (CDRH3) regions of HIV-1 vaccine–elicited Env- and CD4bs-specific Ig repertoires revealed that the CD4bs-specific Ig repertoire displayed overall increased CDRH3 length ($^{****}p < 0.0001$, one-way ANOVA; Fig. 2A) with skewed length distribution than the Env-specific and total IgG repertoire. CD4bs-specific Abs isolated from HIV-infected individuals also displayed longer CDRH3 length (35–37), which could facilitate accessing the epitope including the CD4 binding loop on gp120 situated in a recessed position (37, 38). The CDRH3 length of CD4bs-specific Ig repertoire also has a more confined distribution, ranging from 10 to 25 (mean = 17) aa residues (Fig. 2A), whereas that of the Env-specific repertoire was broader, ranging from 6 to 32 (mean =

15.5) residues (Fig. 2A). Compared with the total Ig repertoire recovered from memory B cells with an average of 14.4 residues of CDRH3 length (17), both the Env and the CD4bs-specific Ig repertoires recovered here had an overall longer CDRH3 (****$p < 0.0001$, one-way ANOVA; Fig. 2A). In contrast, there was no difference in L chain CDR3 lengths between the Env- and CD4bs-specific Ig repertoires ($p > 0.05$, Mann–Whitney test) (Supplemental Fig. 1A). This observation is consistent with the notion that the CDRH3 is the primary determinant for Ag recognition. In addition, there was no significant difference in mean of CDRH3 lengths in sequences isolated at Imm 2 time point compared with those isolated at Imm 5 in either the Env- or CD4bs-specific repertoires (data not shown), suggesting that the CDRH3 length is relatively stable during the course of immunization.

We also observed another unique feature of CD4bs-specific repertoire, the increased degree of hydrophobicity (****$p < 0.0001$, one-way ANOVA) (GRAVY score, Fig. 2B) in the CD4bs-specific CDRH3 regions, which was attributed to a higher content of the hydrophobic amino acid residues F, L, V, I, and M (*$p < 0.05$, one-way ANOVA) compared with the Env-specific and the total Ig repertories (Fig. 2C), partly explained by the prevalent usage of JH5 segment (Fig. 1B). The higher CDRH3 hydrophobicity displayed by the vaccine-elicited CD4bs-specific Ig repertoire is consistent with CD4bs-specific mAbs isolated from natural infection, which interact with the receptor binding site and possess a high degree of hydrophobicity (39).

Furthermore, the positively charged amino acid residues, arginine (R) and lysine (K), were preferentially located in the CD4bs-specific CDRH3 (*$p < 0.05$, Fig. 2C), suggesting that they are responsible for the recognition of the negatively charged CD4 binding loop of gp120 (38), including the critical CD4bs residues on the gp120 target, D368 and E370.

Affinity maturation progressively occurs as evidenced by the elevated levels of SHM during the immunization course

To investigate the Ab affinity maturation process, we queried the amplified Ig sequences against the macaque Ig germline database to assess the level of SHM (18). Both Env- and CD4bs-specific Ig repertoires isolated after Imm 5 displayed ~2% more VH mutations at the nucleotide level and ~4% at the amino acid level, compared with the amplicon sequences after Imm 2 (****$p < 0.0001$, one-way ANOVA) (Fig. 3A). Similar findings were observed for the CD4bs-specific repertoire L chain (V genes of both κ and λ chains, ****$p < 0.0001$, one-way ANOVA) (Supplemental Fig. 1B). The higher level of SHM in the later stage of repeated immunization indicates that affinity maturation occurs progressively over the course of immunization. Upon closer examination of the regions of V-gene segment use for H chains, we found that the mutations within all of the subdomains of the VH region (FR1–3 and CDR1–2) increased from Imm 2 to Imm 5 (**$p < 0.01$, ***$p < 0.001$, ****$p < 0.0001$, Mann–Whitney test) (Fig. 3B), indicating that both FRs and variable CDR regions evolve during affinity maturation. Similarly, the mutations in all of the subdomains of V-gene segment of L chains increased during immunization (data not shown). There were no significant differences in SHM for heavy and L chain V genes between the Env- and CD4bs-specific Ig repertoires (data not shown), suggesting the same level of affinity maturation occurs for both repertories.

HIV-1 vaccine–elicited CD4bs-specific Ab affinity maturation is associated with functionality progression

Given the affinity maturation of the Env- and CD4bs-specific Ig repertoire, indicated by the increasing level of SHM of the Ig H/L chain, we sought to investigate whether the elevated level of SHM was associated with improvements in Ab-Ag binding affinity and virus neutralization capacity. We selected 40 additional clones from Imm 2 and Imm 5, along with the Abs cloned earlier in the study to a total of 74 clones to characterize their epitope binding specificity, Ag-binding affinity, and virus neutralization breadth and potency. The selected clones demonstrated the typical CD4bs-specific gp140-F^{hi}/gp140-F-D368R^{lo} binding phenotype, consistent with that we observed previously. We then assessed their binding affinity for gp120 by BLI as described previously (18). We observed that the binding affinities (K_D) of mAbs isolated from Imm 5 were significantly higher than those from Imm 2 (**$p < 0.01$, Mann–Whitney test; Fig. 4A, *left panel*). Interestingly, the off-rates significantly decreased from Imm 2 to Imm 5 (**$p < 0.01$, Mann–Whitney test; Fig. 4A, *right panel*), whereas the on-rates remained relatively constant (Fig. 4A, *middle panel*), suggesting that the increased Ag binding affinity was primarily achieved by enhanced Ab-Ag complex stability, possibly through accumulated SHM. This observation is consistent with the affinity maturation of other Ag-specific Ab responses such as the tetanus toxoid–specific Abs isolated from human subjects vaccinated with tetanus toxoid vaccine (40).

We further analyzed the neutralization capacity of the cloned CD4bs-specific mAbs against a panel of eight neutralization-

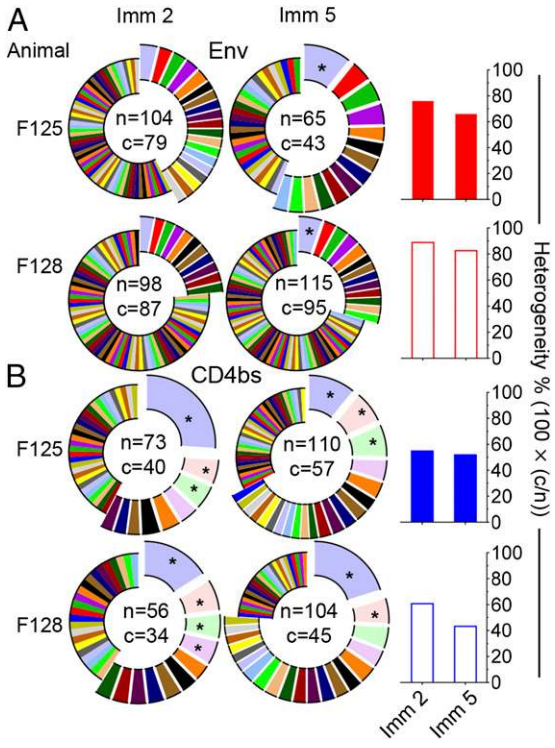

FIGURE 5. The clonal lineages of Env- and CD4bs-specific Ig repertoires display various degrees of heterogeneity at different immunization time points (Imm 2 versus Imm 5). (**A**) The clonal lineage distribution and heterogeneity of single-cell–sorted Env-specific Ig repertoire. Pie charts: each slice of the pie chart represents one clonal lineage (c), with the size of the colored area corresponding to the lineage frequency out of the total number of expansions (n). Clonal lineages with multiple expansions are displayed as exploded portions, lineages that have expanded to constitute >5% of the total number of expansions are marked with asterisks. Bar graph: the heterogeneity (ratio of clonal lineage number [c] to expansion number [n]*100 as [c/n]*100) is summarized on the *right panel* for Env-specific repertoire (red). (**B**) The clonal lineage distribution and heterogeneity of single-cell–sorted CD4bs-specific Ig repertoire, displayed as in (A). The heterogeneity is summarized on the *right panel* for CD4bs-specific repertoire (blue).

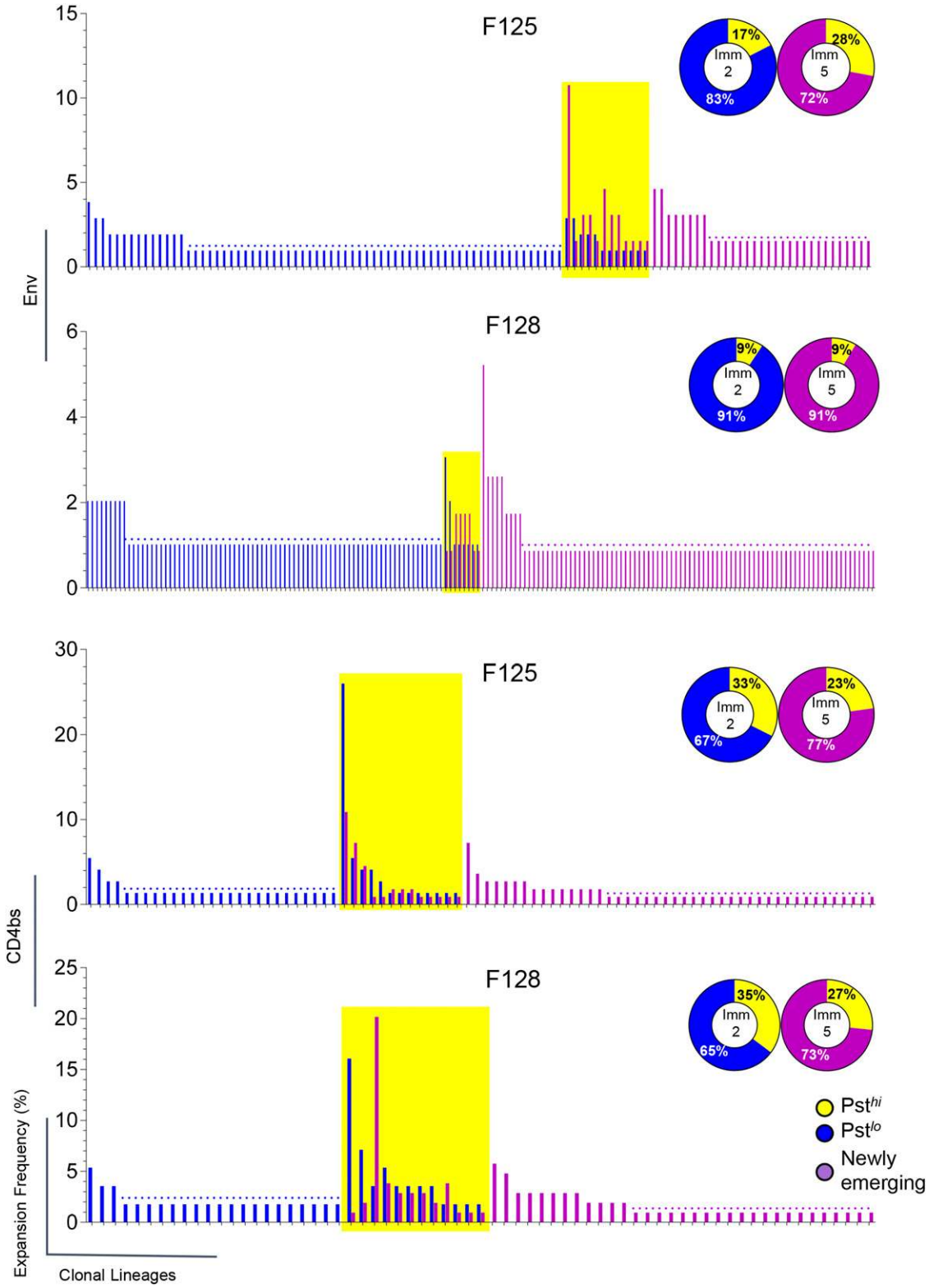

FIGURE 6. Persistent clonal lineages of Env- and CD4bs-specific repertoires from animals F125 and F128 have established during the immunization. Bar graph: the frequency of expansions from each individual clonal lineage at different immunization time points. Clonal lineages isolated at Imm 2 are in blue and Imm 5 in purple. The clonal lineages, which have expansions at both time points, are highlighted with yellow boxes. Dot lines depict the frequency of clonal lineages with single expansion in the repertoire at each time point. Pie chart: the persistence of clonal lineages of the Env- and CD4bs-specific repertories. Clonal lineages that have expansions at both time points are referred to as highly persistent and designated as Pst^{hi} compartment (yellow), that have expansions only at Imm 2 were classified as of Pst^{lo} (blue), whereas lineages that have expansions only at Imm 5 were designated as Newly emerging (purple) compartment. The frequencies of these three categories of clonal lineages with different clonal persistence out of the total clonal lineages were indicated. Env-specific lineages are shown in the *upper two panels* and CD4bs lineages in the *lower two panels*.

sensitive HIV-1 strains (tier 1) including clades A, B, and C pseudoviruses, along with three neutralization-resistant primary strains (tier 2, clade B) (Supplemental Table I). All cloned mAbs displayed various capacities for neutralizing tier 1 viruses, albeit no neutralization against tier 2 viruses was observed (Supplemental Table I). Consistently, the tier 1 virus HXBc2 was preferentially neutralized by most of the CD4bs-specific mAbs (~88% of total cloned mAbs). The allogeneic (nonclade B) tier 1 viruses, DJ263 and MW965, were neutralized by 34 and 22% of these mAbs, respectively (Supplemental Table I). Moreover, the neutralization potency and breadth against tier 1 viruses were found to increase during the course of immunization (**$p < 0.01$, Mann–Whitney test; Fig. 4B, *left* and *middle panels*). Finally, we found that the Ag-binding affinity (K_D) and virus neutralization potency (IC_{50} Geomean) were highly correlated (****$p < 0.0001$, nonparametric Spearman correlation; Fig. 4B, *right panel*), indicating that the improved functionality of CD4bs-specific Abs evolved in parallel with the elevated levels of SHM. Interestingly, CD4bs-specific clones isolated early during the course of immunization (Imm 2) had moderate levels of SHM, Ag-binding affinity, and neutralization potency (Fig. 4C). Somehow, contrastingly, clones at late immunization stage (Imm 5) had broader ranges (from moderate to high) of SHM level, affinity, and neutralization capacity distribution (Fig. 4C), and thus possess higher degree of heterogeneity.

Env- and CD4bs-specific Ig repertoires are diversified with moderate degree of clonal dominance

To gain further insight into how the Env- and CD4bs-specific B cell repertoires evolve during the immunization course at clonal level, we sought to dissect the clonal lineage composition of these repertoires. The clonal lineage was defined using the criteria initially deployed for TCR analysis (41) and subsequently adopted for BCR studies (17, 42), briefly listed as: 1) same V and J gene usage, 2) same CDR3 length, and 3) CDR3 nucleotide sequence homology >90%. Based on this definition, we classified the H chain Ig repertoire into different clonal lineages to first assess the diversity of the repertoire.

We found that the Env-specific Ig repertoire was highly diversified, with the majority of the repertoire consisting of a single clone per lineage, whereas a few lineages consisted of multiple clonal expansions (Fig. 5A, *left*). We observed a similar trend for the CD4bs-specific repertoire (Fig. 5B, *left*), although there were more lineages consisting of multiple clones compared with the Env-specific repertoire. Notably, occasionally there were predominant clonal lineages with expansion frequencies accounting for >5% of the total repertoire in both repertoires (marked with asterisk) (Fig. 5, *left panels*). The heterogeneity of each respective repertoire was further assessed by the ratio of the number of clonal lineages (c) to the total number of expansions (n). In summary, the Env-specific repertoire displayed a higher degree of heterogeneity (>60%) (Fig. 5A, *right upper panel*) than the CD4bs-specific repertoire (40–50%) (Fig. 5B, *right lower panel*), which is consistent with that the Env-specific repertoires recognize more diversified epitopes than the relatively focused CD4bs-specific repertoires. There was a slight decrease of heterogeneity in both repertories from time point Imm 2 to Imm 5 (Fig. 5, *right panels*). However, given the limited sampling numbers, it is not clear whether this observed decrease in heterogeneity is significant.

Similarly, the Ig L chain amplicons were also analyzed for clonal lineage compositions with >50 and 30% heterogeneity detected for the Env- and CD4bs-specific repertoires, respectively (data not shown). Together, the Env- and CD4bs-specific Ig repertoires were highly diversified with moderate portion of predominant lineages.

Persistent clonal lineages exist in both of the Env- and CD4bs-specific Ig repertoires

The clonal lineage classification of the Env- and CD4bs-specific Ig repertoires allowed us to longitudinally interrogate their level of prevalence (defined as the frequency of all expansions from a given clonal lineage within the entire repertoire) at different immunization time points. We observed that a small but notable portion of lineages consists of expansions identified at both Imm 2 and Imm 5 repertoires (Fig. 6, *left*, yellow), whereas the majority of the clonal lineages were only identified at one of the time points (Fig. 6, *left*, blue or purple). Based on the frequency of each clonal lineage within the whole repertoire along the immunization course, we classified them into three types according to their different degree of clonal persistence: 1) high persistence (Pst^{hi}), with expansion present at both Imm 2 and Imm 5 time points (Fig. 6, *right*, yellow); 2) low persistence (Pst^{lo}), with expansion present only at Imm 2 (Fig. 6, *right*, blue); and 3) newly emerging, with expansions present only at Imm 5 (Fig. 6, *right*, purple). The latter type was most likely activated after the Imm 2. The existence of the

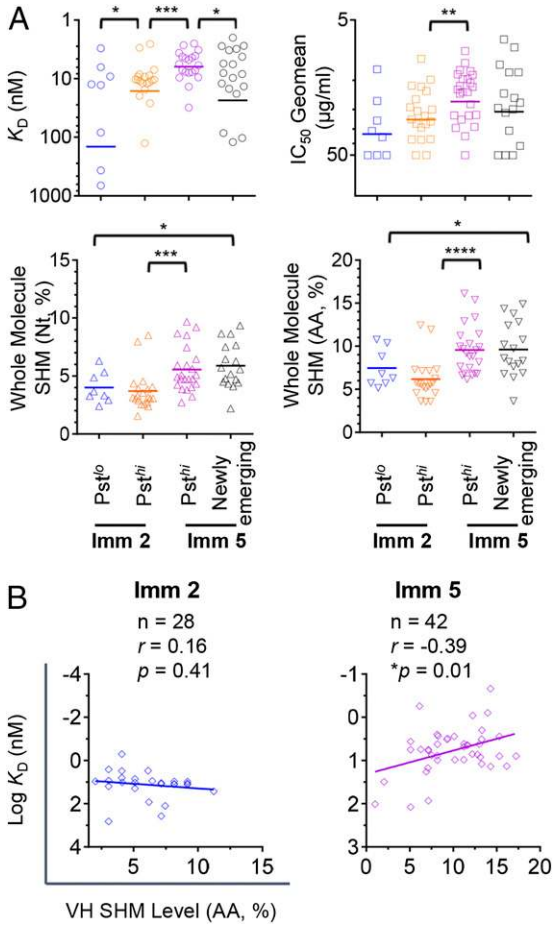

FIGURE 7. Affinity selection is strongly associated with clonal persistence of CD4bs-specific repertoire. (**A**) Genetic and functional characterization of clones from the Pst^{hi}, Pst^{lo}, and Newly emerging lineages in the CD4bs-specific repertoire. The statistical differences of binding affinity K_D (*upper left panel*), neutralization potency (*upper right panel*), SHM nucleotide level (*lower left panel*), and amino acid level (*lower right panel*) between each two of the four compartments were evaluated using one-way ANOVA or Mann–Whitney test. *$p < 0.05$, **$p < 0.01$, ***$p < 0.001$, ****$p < 0.0001$. (**B**) The correlation between binding affinity (transformed K_D log) and VH amino acid SHM level was determined at Imm 2 (*left panel*) and Imm 5 (*right panel*), respectively, using the nonparametric Spearman test.

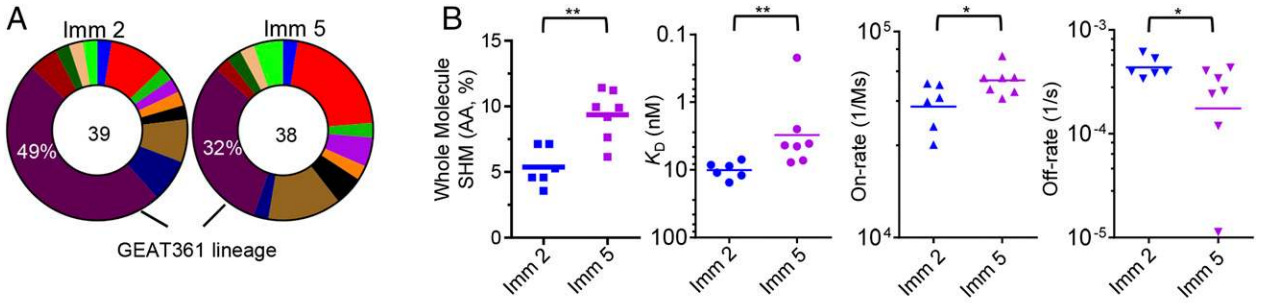

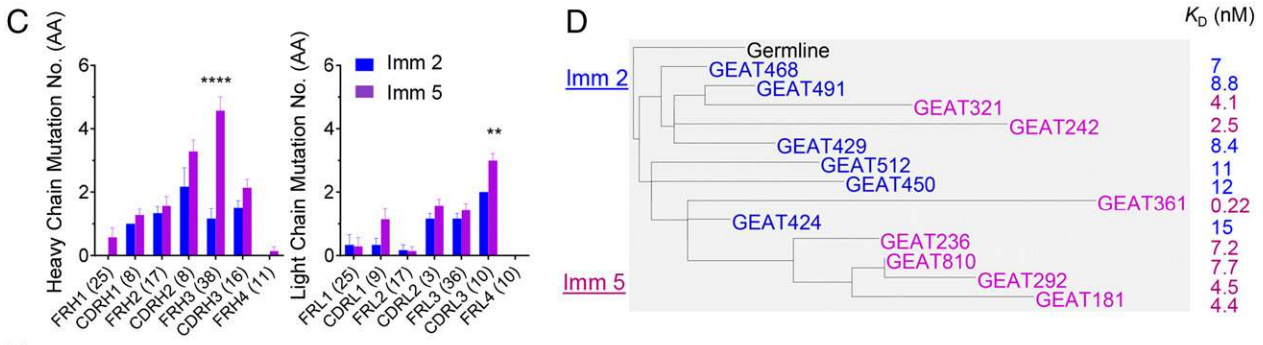

E

	Clade	Virus	mAb at Imm 2						mAb at Imm 5							human mAb
			GEAT 424	GEAT 429	GEAT 450	GEAT 468	GEAT 491	GEAT 512	GEAT 181	GEAT 236	GEAT 242	GEAT 292	GEAT 321	GEAT 361	GEAT 810	VRC01
Tier 1	B	HXBc2	2.18	1.32	0.66	0.55	2.14	1.21	0.51	1.19	1.1	0.42	0.53	1.59	0.52	0.02
	B	MN	1.69	0.19	0.24	0.22	0.64	0.14	0.23	0.05	0.44	0.1	0.07	0.45	0.23	0.02
	B	SF162	>50	>50	14.2	>50	>50	>50	11.7	7.07	31.6	6.69	6.91	9.78	6.82	0.13
	B	SS1196	>50	>50	ND	ND	>50	>50	24.6	>50	>50	13.5	>50	>50	19.6	0.25
	B	BaL.26	>50	>50	>50	>50	>50	>50	>50	>50	>50	>50	>50	>50	>50	0.03
	B	JRCSF	>50	>50	ND	ND	>50	>50	>50	>50	>50	>50	>50	>50	>50	0.08
	A	DJ263.8	>50	>50	>50	>50	15.9	>50	8.05	12.6	16	15.7	6.01	16	>50	0.08
	C	MW965.26	>50	>50	25.2	>50	>50	>50	0.08	>50	0.23	>50	>50	0.05	>50	0.04
Tier 2	B	JRFL	>50	>50	>50	>50	>50	>50	>50	>50	>50	>50	>50	>50	>50	0.02
	B	89.6	>50	>50	>50	>50	>50	>50	>50	>50	>50	>50	>50	>50	>50	0.53
	B	YU2	>50	>50	>50	>50	>50	>50	>50	>50	>50	>50	>50	>50	>50	0.2
	Tier 1 geomean		22.1	15.8	7.2	9.6	17	15	3.9	8.7	7.2	7.2	7.5	5.4	10	0.06
	Tier 1 breadth		25	25	67	33	38	25	75	50	63	63	50	63	50	100

IC_{50} (μg/ml): <1 1-50 Note: ND: no determined.

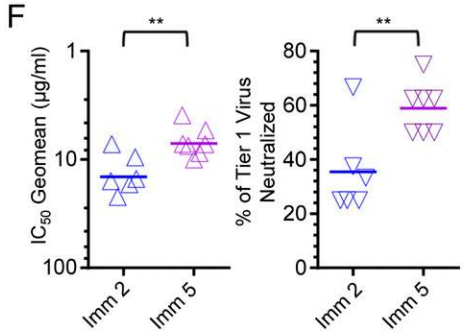

FIGURE 8. The affinity maturation pathway of a predominant persistent CD4bs-specific clonal lineage. (**A**) The clonal composition of the highly persistent lineages (Pst^{hi}) in the CD4bs Ig repertoire from animal F125. The expansion frequency (percent) of each CD4bs-specific Pst^{hi} clonal lineage out of the total Pst^{hi} compartment is color coded and illustrated with the total expansion numbers of the Pst^{hi} compartment, indicated in the center of the pie chart. One of the most dominant clonal lineages, namely, GEAT361 lineage, possesses the highest expansion frequencies of 49 and 32% at Imm 2 and 5 time points, respectively, and is marked and selected for further characterization. (**B**) SHM and binding affinity (dissociation constants [K_D], association [on-rate], and dissociation [off-rate] rates) of clones from the GEAT361 lineage at Imm 2 and Imm 5 time points (*t* test; $*p < 0.05$, $**p < 0.01$). (**C**) Average accumulated mutations within the H and L chain subdomains of variant clones within the GEAT361 lineage at time point Imm 2 and Imm 5, respectively (two-way ANOVA; $**p < 0.01$, $****p < 0.0001$). (**D**) Phylogenetic analysis of the Ig molecules of the selected variant clones in the GEAT361 lineage. Both the H chain VDJ sequence and the matched L chain VJ sequence were used to generate the phylogenetic tree of the whole Ab molecule from both Imm 2 (blue) and Imm 5 (purple) time points with the germline precursor molecule colored in black. The corresponding mAb binding affinity (K_D) to gp120 is also displayed on the *right side*. (**E**) The neutralization capacity of the selected variant clones of GEAT361 lineage isolated at Imm 2 (blue) and Imm 5 (purple), respectively, were tested to neutralize a panel of HIV-1 pseudoviruses from different clades. Virus neutralizing (*Figure legend continues*)

Pst^{hi} clonal lineages accounted for ~9–28% of the Env-specific and 23–35% of the CD4bs-specific repertories, respectively (Fig. 6, *right*), which are substantial portions.

Because it is possible that the prevalence of certain clonal lineages may be below the level of detection in the repertoires generated by single-cell sorting, because of their low frequencies in the total B cell repertoire or sample limitations, we interrogated the presence of the representative clonal lineages by querying their related sequences in a more comprehensive repertoire generated by B cell NGS to overcome the depth limitation imposed by single-cell sorting (17). We found that, consistent with our clonal lineage classification based on a single-cell sorting method, the Pst^{hi} clonal lineages always present at a higher frequency (~3-fold) of expansions than the Pst^{lo} clonal lineages for both Env- and CD4bs-specific repertoires (Supplemental Fig. 2). Furthermore, we constantly observed recurring isolation of most of (~70%) CD4bs-specific memory B cells from the same clonal lineage in independent single-cell–sorting experiments using the same PBMC sample. Therefore, the clonal lineage persistence classification based on the clonal prevalence sampled by single-cell sorting properly illustrated the repertoire clonal durability.

Affinity for Ag plays a critical role in determining clonal lineage persistence

To investigate the genetic properties of the clonal lineages with Pst^{hi}, we asked whether the SHM level of the clones from the CD4bs-specific lineages primarily determined their degree of persistence. We found that at the same immunization time point, there was no significant difference in SHM levels between the clones in the Pst^{hi} and the Pst^{lo} or Newly emerging lineages at both the nucleotide and the amino acid levels (data not shown).

To investigate the functional properties associated with Pst^{hi} clonal lineages, we selected representative Ig sequences from each cluster of the Pst^{hi}, Pst^{lo}, and the Newly emerging lineages for further analysis. Interestingly, clones from the Pst^{hi} lineages displayed significantly higher gp120 binding affinity than the clones from Pst^{lo} or Newly emerging lineages at the same immunization time point (Imm 2 or Imm 5) ($*p < 0.05$, Mann–Whitney test; Fig. 7A, *upper left panel*), which indicates that CD4bs-specific memory B cell clones with high binding affinity to gp120 at the early immunization time point are more likely to persistently evolve and expand. Within the Pst^{hi} clonal lineages, increasing gp120 binding affinity was also associated with elevated neutralizing potency from Imm 2 to Imm 5 ($**p < 0.01$, one-way ANOVA; Fig. 7A, *upper right panel*). Consistent with the observation of the total CD4bs-specific repertoire, the selected mAbs demonstrated no significant difference in SHM at either nucleotide or amino acid levels at the same immunization time point (Fig. 7A, *lower panels*).

In light of the observation that it is the Ag affinity, not SHM, that drives Ab persistence, we examined the correlation between the VH SHM level and affinity for Ag gp120 of each CD4bs-specific Ab clone. We found that such correlation varied between different immunization time points. At early immunization time point (Imm 2) when the overall SHM level of the repertoire was low, there was no correlation between the SHM level and the Ab affinity for gp120 (Fig. 7B, *left panel*). In contrast, at later immunization time point (Imm 5) with overall increasing SHM level, there was a correlation between the SHM level and the Ab affinity for the Ag ($*p < 0.05$, nonparametric Spearman correlation; Fig. 7B, *right panel*). Overall, our data suggest that: 1) at early immunization time point, clonal lineage persistence is determined by Ag affinity selection, less dependent on SHM levels; and 2) once clonal lineage persistence is established, the accumulated SHM results in elevated Ag affinity. Our data reinforce the critical role Ag affinity selection plays during the early immunization time point in determining the clonal persistence of desirable clonal lineages including that of the bNAbs.

The affinity maturation of a predominant CD4bs-specific clonal lineage of Pst^{hi}

In this study, we observed that CD4bs-specific clonal lineages displayed various degrees of clonal persistence and predominance. There was occasional occurrence of clonal lineages with Pst^{hi} and moderate predominance (Fig. 5). To gain insight into the affinity maturation process of the highly persistent and predominant clonal lineages, we selected the most predominant CD4bs-specific persistent clonal lineage of the repertoire of animal F125, the GEAT361 lineage, to investigate its genetic and functionality evolution. GEAT361 lineage expansions accounted for 49 and 32% of the total Pst^{hi} expansions identified by single B cell sorting from animal F125 at Imm 2 and 5 time points, respectively (Fig. 8A). This clonal lineage uses VH4.22_JH5 with 16-aa residues in CDRH3 and VL2.13_JL3 with 10-aa residues in CDRL3. Representative Abs within this clonal lineage were cloned and their binding specificities to the CD4bs were verified (Supplemental Fig. 3A).

Consistent with our early observation, clones of GEAT361 lineage at Imm 5 displayed significantly higher SHM level of both VH/VL chains and binding affinity (both on-rates and off-rates) than those at Imm 2 ($*p < 0.05$, $**p < 0.01$, *t* test; Fig. 8B). Upon closer investigation of SHM mutations in VH and VL subdomains (Supplemental Fig. 3B), we found that the most prominently accumulated mutations occurred within FR3 of the H chain ($****p < 0.0001$, two-way ANOVA) and CDR3 of the λ-chain ($**p < 0.01$, two-way ANOVA) from Imm 2 to Imm 5 (Fig. 8C). Interestingly, we found that a loop region within the H chain FR3 subdomain, which connects the strands D and E of FR3 (IMGT definition), and is referred to as TCR HV4-like region (43–45), or sometimes as CDR4, contained high levels of SHM (Supplemental Fig. 3B). The HV4-like loop region of IgH FR3 usually is in the same plane with the H chain CDRs (46) and could contribute to Ag recognition or interaction with super Ags (46–48). To examine the spatial distribution of the residues of SHM within the FR3 subdomain, we modeled the structure of the VH region of GEAT361 lineages using the CD4bs-specific mAb GE136 Fab as template to reveal the approximate three-dimensional locations of these residues (Supplemental Fig. 3C). In this model, we found that most of the FR3 residues modified by SHM are distal from the CDRs, whereas some of the mutations within the HV4-like region are proximal to the CDRs (Supplemental Fig. 3C) and could directly contribute to Ag binding affinity. In summary, our data suggest that the overall increasing affinity for Ag is likely caused by accumulated SHM in the Ab molecule, particularly enriched in both of the FRs of the VH and V region of the VL gene.

Consistently, phylogenetic analysis of the whole molecular sequences revealed that clones at Imm 2 segregated into clusters

potency was color-coded as indicated, and tier 1 virus neutralization Geomean and breadth were calculated with CD4bs bNAb VRC01 as reference Ab. (**F**) Comparison of the tier 1 virus neutralization potency (IC_{50} Geomean) and breadth (% of tier 1 viruses neutralized) between the CD4bs mAbs isolated from Imm 2 and Imm 5 time points (*t* test; $**p < 0.01$).

A

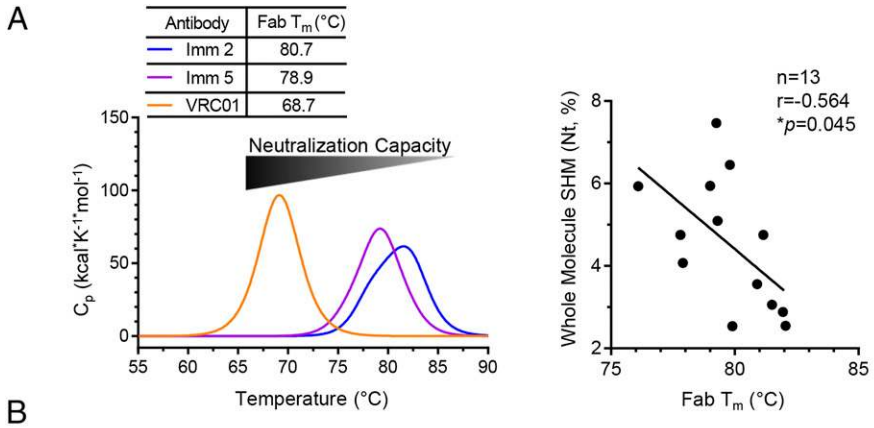

B

	gp120 region		Mutation	Imm 2 GEAT 424	Imm 2 GEAT 468	Imm 2 GEAT 429	Imm 2 GEAT 450	Imm 5 GEAT 181	Imm 5 GEAT 321	Imm 5 GEAT 361	Imm 5 GEAT 810	control mAbs CD4-Ig	F105	VRC01	2G12	HIVIg
			WT gp120	100	100	100	100	100	100	100	100	100	100	100	100	100
Inner domain		V2	D167N	102	74	83	66	73	67	82	65	83	196	84	100	122
		V1/V2 stem	N197T	63	40	40	64	30	30	30	30	30	21	79	100	104
	C2	β9	N262A	32	13	11	20	86	8	105	14	0	136	24	100	108
		Loop D	D279A	107	132	138	105	100	113	133	117	37	111	0	100	63
	V3	V3 base	N332A	148	157	113	150	101	125	96	102	118	45	113	6	100
			S365A	206	220	135	226	139	144	151	203	173	91	209	100	78
			G366A	90	103	104	73	71	88	89	64	11	97	47	100	128
			G367A	81	132	113	92	106	116	120	162	1	121	29	100	103
			D368A	8	19	0	0	14	0	10	2	1	0	18	100	133
	C3	CD4 binding loop	P369A	73	44	68	41	64	51	87	49	58	88	82	100	110
			E370A	13	25	20	17	43	33	86	9	0	1	33	100	60
			I371A	30	31	24	24	143	24	109	24	5	2	33	100	71
			V372A	143	260	199	204	184	213	200	144	94	254	87	100	72
			M373A	125	251	154	163	136	148	162	120	91	139	76	100	69
Outer domain		β19	K421A	37	97	22	60	32	45	62	44	103	42	129	100	123
	C4	β20/21	N425A	193	203	169	165	197	171	176	89	13	137	79	100	70
			W427A	91	82	75	86	120	103	113	152	0	149	85	100	57
		β23	D457A	142	105	79	108	79	83	86	78	1	81	35	100	88
	V5	V5/β24	I467A	161	152	104	137	133	100	121	159	97	115	51	100	116
			R469A	199	212	136	187	146	141	133	259	4	151	78	100	112
			G471A	228	238	136	214	159	150	162	238	157	85	166	100	116
		β24/α5 connection	G472A	124	167	123	84	116	103	118	128	1	78	81	100	92
			G473A	167	212	157	129	124	165	98	132	0	14	73	100	103
	C5		D474A	0	0	23	0	15	15	27	0	48	0	23	100	87
			M475A	271	186	157	144	191	194	168	132	46	ND	151	100	90
		α5	R476A	24	333	216	237	131	221	177	142	44	136	76	100	110
			W479A	7	84	84	5	2	2	84	3	1	27	84	100	102

C

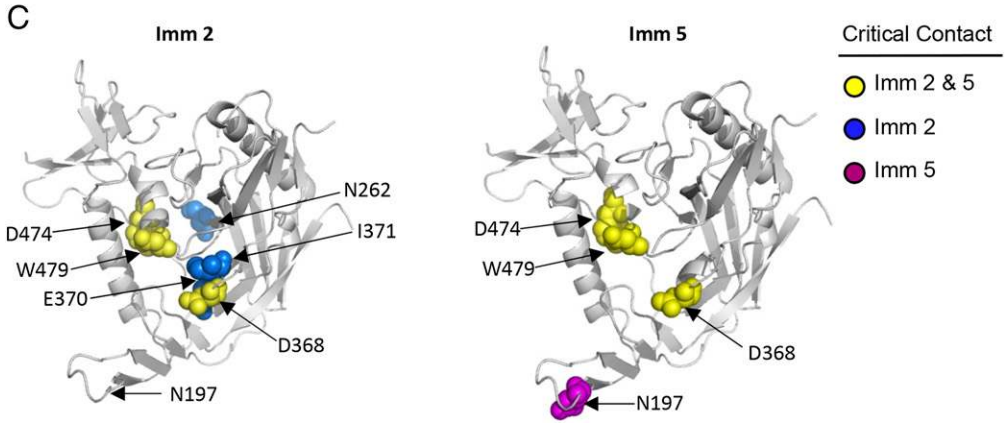

FIGURE 9. GEAT361 lineage thermostability and footprints shift from Imm 2 to Imm 5. (**A**) The Ab affinity maturation is associated with the change of thermal stabilities of the free Ab molecule. *Left*, The average DSC melting profiles of the Fab portion of the mAbs (Fab T_m) from the Imm 2 (blue) and Imm 5 (purple) time points. Note that from Imm 2 to Imm 5 time point, the average Fab T_m decreases, conversely with the increasing trend of Ab affinity for gp120 and virus neutralization capacity. The bNAb VRC01 (orange) has an even lower Fab T_m. *Right*, Correlation between the whole molecule SHM (nucleotide [Nt]) and the Fab T_m of the cloned mAbs (nonparametric Spearman test). (**B**) Representative clones from the GEAT361 linage and selected human Abs as references were tested to bind a panel of JRCSF Env mutants containing single Ala point mutations in gp120. Both 2G12 and HIVIg served as controls. The effect of Ala mutation on Ab binding is shown relative to WT gp120. A 3-fold reduction by mutation was highlighted in blue and a 3-fold increase highlighted in red. (**C**) gp120 core surface (Protein Data Bank: 2NY3) used to highlight the recognition sites on gp120 by selected GEAT361 clonal variants inferred by Ala scanning. *Left*, Footprints of Imm 2 mAb variants of lower-affinity maturation level. *Right*, Footprints of (*Figure legend continues*)

closer to the germline precursor sequence (Fig. 8D, blue) with overall lower affinity (Fig. 8D, greater K_D value) than those at Imm 5 (Fig. 8D, lower K_D value, purple), which form clusters in more distal positions from the inferred germline precursor (Fig. 8D). These data demonstrated that for HIV-1 CD4bs-specific Pst^{hi} predominant clonal lineages, the increased genetic divergence from the assigned germline ancestor (level of SHM) from Imm 2 to Imm 5 was associated with elevated affinity for cognate Ag.

We also characterized the virus neutralization capacity of the mAbs from this lineage (Fig. 8E) and found that its viral neutralization potency and breadth also elevated from Imm 2 to Imm 5 (**$p < 0.01$, t test; Fig. 8F). Interestingly, although the neutralization breadth of mAb clones isolated from Imm 2 was overall restricted within clade B tier 1 viruses, most of the mAb clones isolated from Imm 5 possessed the capacity for neutralizing clade A virus DJ263.8 and some of them neutralized clade C virus MW965.26 at high potency (Fig. 8E). Three mAbs isolated from Imm 5, GEAT181, 242, and 361, which displayed higher Ag affinity and SHM (Fig. 8D), demonstrated superior neutralization breadth and potency against these selected viruses (Fig. 8E). These data indicate that the affinity maturation process leads to improved cross-clade virus neutralization.

Ab affinity maturation pathway involves decreased thermostability and moderately shifted footprint on gp120 surface

The substantial effects of somatic mutations within Ab H/L chain framework subdomains on the Ag binding affinity and virus neutralization capacity of the Ab may result from the improved thermodynamic folding of Ab molecules. Thus, we assessed the thermostability of the fragment Ag-binding (Fab) portions of selected mAbs from this GEAT361 lineage by DSC. Interestingly, we found the melting temperature (T_m) of Fab portions of the Imm 2 mAbs (T_m = 80.7˚C) displayed ~2˚C higher than that of the Imm 5 mAbs with T_m = 78.9˚C (Fig. 9A, *left panel*). Referring to the human bNAb, VRC01 with an average SHM of 25% as a whole molecule (28) and a fairly low T_m of 68.7˚C (Fig. 9A, *left panel*), we speculated that Abs with higher SHM may lose thermostability. As expected, we observed a negative correlation between the thermostability (Fab T_m) and SHM (*$p < 0.05$, nonparametric Spearman correlation) (Fig. 9A, *right panel*). Therefore, during Ab affinity maturation with elevated Ag recognition affinity, the thermostability of the free Ab molecule could decrease as the cost of Ag affinity selection.

To understand how accumulated SHM affects the Ab affinity and virus neutralization capacity, we investigated whether somatic variants from different immunization time points display different footprints on the surface of Ag gp120. We tested the apparent binding affinity of the representative clones from both time points with a panel of alanine scanning mutants of the gp120 of virus isolate JRCSF by ELISA assay. Shown in Fig. 9B, with a panel of known CD4bs-specific mAbs as references, we were able to compare the footprints of these mAb variants. As typical CD4bs-specific Abs, all clones had abolished binding affinity to gp120 variants with the mutations in the CD4 binding loop (D368A) and β24/α5 connection (D474A) (Fig. 9B), suggesting that the interaction interface between the Ab and these two major recognition regions of gp120 were established by time point Imm 2.

In addition, we found that the mutations on the V1/V2 stem (N197T), β9 (N262A), and CD4 binding loop (E370A and I371A) of gp120 surface displayed different effects on the gp120 binding affinity for mAbs at these two different time points (Fig. 9C). In general, from Imm 2 to Imm 5, the effect of V1/V2 stem mutation N197T on Ab binding affinity to gp120 greatly increased, suggesting that the Imm 5 Abs have increased contact with V1/V2 stem (Fig. 9C). For the clones GEAT181 and 361, isolated from Imm 5 with the best neutralization breadth (Fig. 8E), there were profound differences in their footprints in CD4 binding loop (E370 and I371) and β9 (N262) compared with the other somatic variants (Fig. 9C). Such footprint differences on gp120 may confer to the expanded tier 1 virus neutralization breadth and was established later during the immunization regimen through accumulated SHM. Consistent with the tier 1 virus–restricted neutralization capacity, the footprints of the selected clones in the clonal lineage evolved during the course of immunization were similar to the footprints of the non-bNAb, F105, distinct from the footprints of the bNAb, VRC01 (Fig. 9B) (49).

Discussion

To efficiently elicit CD4bs bNAb response in a vaccine setting, it is important to understand the mechanistic evolution of CD4bs-specific Ab responses by vaccination. Questions remain unclear in the field about the degree of diversity, durability, and persistence of the response elicited by Env vaccine candidates. In this study, we focused on the developmental pathways of CD4bs-specific Ig repertoire during the immunization course of NHPs immunized with the first generation of soluble trimeric form of Env immunogen, gp140-F. We investigated the genetic composition and functional evolution of CD4bs-specific Ig repertoire responses, including gene segment usage preference, clonality delineation, as well as the role of SHM and affinity selection on clonal lineage evolution to fill the knowledge gaps. Although tier 2 neutralizing Ab responses targeting the CD4bs have not yet been elicited after Env vaccination, in this study we establish the foundations of a high-resolution analytical system that will be of high value as our capacity increases to efficiently elicit such responses in NHPs.

The CDRH3 regions confer the fine specificity of Abs. Strikingly, ~80% of the CD4bs-specific Ig repertoire displays CDRH3 length from 15 to 19 (mean, 17) residues, whereas the CDRH3 lengths of most Env-specific Abs possess a broader range from 12 to 19 (mean, 15.5) residues, as do Abs comprising the total IgG repertoire (mean, 14.4). The CDRH3 sequences of the CD4bs-specific Ig repertoire are more hydrophobic and also contain more positively charged residues than those of Env-specific repertoire. The unique CDRH3 features of CD4bs-specific Ig repertoire are under pressure of functional selection, which is consist with the result from a recent study that demonstrated that DH germline origins could profoundly influence Ab recognition (50).

During the immunization course, both CD4bs- and Env-specific Ig repertoires display substantial increasing levels of SHM, Ag binding affinity, and improved virus neutralization capacity limited to tier 1 viruses. We observed that mAb binding affinity was significantly associated with neutralization potency against tier 1 viruses (Fig. 4B, *right panel*), suggesting mAbs with higher binding affinity possess more efficient neutralization capacity. We also found that the increasing Ag-binding affinity during the im-

the variants with the highest degree of affinity maturation, GEAT181 and 361, isolated from Imm 5 time point. gp120 backbone is in gray and residues affecting Ab binding for both Imm 2 and Imm 5 variants are highlighted in yellow, whereas mutations on residues only affecting binding at Imm 2 or Imm 5 are highlighted in blue and purple, respectively.

munization course (Fig. 4A) correlated with the decreases in Ab-Ag complex dissociation rates (off-rate), presumably because of the accumulation of the interactions within the Ag-Ab recognition interface possibly caused by SHM. The Imm 5 CD4bs repertoires display higher degree of heterogeneity in terms of the SHM level, affinity for Ag, and tier 1 virus neutralization capacity than that of Imm 2 (Fig. 4C). Therefore, it appears that the repeated immunization with the same immunogen continuously drives affinity maturation for persistent clonal lineages, while recruiting newer clones and maintaining the clonal diversities of the B cell repertoire.

Memory B cell clonal lineages of both Env- and CD4bs-specific Ig repertoires undergo dynamic evolution during the immunization course and display various degrees of persistence. A notable portion of the CD4bs-specific clonal lineages displayed a high degree of persistence and maintained substantial population sizes. Interestingly, we found that Ag affinity selection plays a primary role in determining clonal lineage persistence. The administered immunogen in this study is likely in favor of the clonal lineages with relatively high Ag cognate affinity leading to the efficient clonal expansion, which subsequently maintains Pst^{hi}. As demonstrated in our previous study, the imperfect antigenicity of the gp140-F immunogen resulted in the elicitation of CD4bs-specific B cell responses with limited neutralization capacity because of suboptimal binding angles and footprints (18, 51). However, the strong association of Ag affinity and lineage persistence shown in this study provides hope that recently developed well-ordered Env trimers will likely lead to the elicitation of Ab responses with improved neutralizing capacity in the future (7, 52).

Characterization of a representative predominant persistent CD4bs-specific clonal lineage revealed that SHM in both FRs and CDR regions of Ig molecule contributed to the functionality evolution, including the overall increased Ab binding affinity to cognate immunogens, decreased thermostability, and subtle shifts in Ab footprints on the cognate Env gp120 surface, as well as the virus neutralization breadth against heterologous viruses. It is possible that the accumulated SHM during affinity maturation leads to a higher degree of Ig molecular flexibility, which favors Ag-Ab–induced fit and complex stability. This observation is consistent with the limitations of Ag affinity evolution previously reported in a tetanus toxoid vaccination study (40). Extensive SHM accumulated in the HIV-1 Env-specific Abs frameworks that are critical for virus neutralization breadth and potency has been observed in Ab repertoires elicited during natural infection (53). The accumulated SHM associated with functionality within the H chain FR3 of Abs, including the HV4-like region, highlights the potential of this subdomain to modulate Ag recognition. Compared with the observed considerable SHM within the H chain FRs and L chain CDRs, CD4bs-specific Ig repertoire CDRH3 were relatively consistent during the immunization course (Fig. 8C, Supplemental Fig. 3B), with minimal changes, suggesting that CDRH3 predominantly conferring Ab specificity is mostly predetermined.

Despite the great genetic diversity of the CD4bs-specifc B cell repertoire, we observed a few predominant clonal lineages in the persistent compartment from these two immunized animals, which accounted for >5% of the sampled repertoire. The persistent CD4bs-specific B cell repertoire of animal F125 consisted of predominant H chain VH4.22_JH4/5_CDRH3 16 aa, which used L chains of either VL2.13_JL3_CDRL3 10 aa or VL2.7_JL2_CDRL3 10 aa (data not shown). We also observed that H chain VH4.11_JH5_CDRH3 18 aa usage is predominant in the persistent CD4bs-specific repertoire, with L chain VL2.7_JL2_CDRL3 10 aa usage in animal F128 (data not shown). Therefore, L chain clonal lineage, VL2.7_JL2_CDRL3 10 aa, commonly used by the repertoires from both animals, together with H chain clonal lineages of VH4.11_JH5_CDR3 18 aa and VH4.22_JH4/5_CDR3 16 aa, might be common signatures for rhesus monkey CD4bs-specific B cell clones.

It is not surprising that footprints of the persistent predominant GEAT361 lineage isolated from animal F125 resemble the non-bNAb F105 more than the bNAb, VRC01 on gp120 surface (Fig. 9B), in light of the overall moderate virus neutralization breadth of the serum from animal F125 (22). It has been increasingly appreciated that the model immunogen, YU2gp140-F, exposed antigenic Env surfaces that are not exposed on the native functional Env spike, explaining the elicitation of non-bNAbs (51). However, by using an immunization regimen based on purified glycoprotein in adjuvant in this study, we were able to robustly elicit total Env- as well as CD4bs-specific memory B cell responses, with ~5% memory B cells being Env-specific and ~5% of Env-specific memory B cells being CD4bs-specific by flow cytometry. Furthermore, the strong correlation of SHM, affinity for cognate Ag, and virus neutralization capacity of the highly persistent predominant CD4bs-specific clonal lineage elicited by vaccination suggest that it is feasible to elicit persistent Ab responses to conserved determinants with the next generation of HIV-1 trimeric Env vaccine candidates that display improved antigenicity (5–7) at protective titers in the future.

In conclusion, our data demonstrate that affinity maturation of the CD4bs-specific Ig repertoire occurred progressively and clonal lineage persistence is achievable with Env vaccine immunization in NHPs. Among different individual immunized NHP animals, there are CD4bs-specific clonal lineages of Pst^{hi} with notable genetic convergence, which have important implication for vaccine development.

Acknowledgments

The following reagents were obtained through the National Institutes of Health AIDS Reagent Program, Division of AIDS, National Institute of Allergy and Infectious Diseases, National Institutes of Health: anti–HIV-1 gp120 Abs including 2G12 from Dr. Hermann Katinger, 39F from Dr. James Robinson (Tulane University), F105 from Dr. Marshall Posner (Dana Farber Cancer Institute), and HIVIg. We are grateful to Dr. Joseph Sodroski (Dana Farber Cancer Institute) for providing the plasmid encoding CD4-Ig and Dr. Dennis Burton (The Scripps Research Institute) for providing JRCSF gp120 alanine scanning mutant panel plasmids. We thank James Steinhardt for proofreading this manuscript.

Disclosures

The authors have no financial conflicts of interest.

References

1. Lewis, G. K., A. L. DeVico, and R. C. Gallo. 2014. Antibody persistence and T-cell balance: two key factors confronting HIV vaccine development. *Proc. Natl. Acad. Sci. USA* 111: 15614–15621.
2. Burton, D. R., and J. R. Mascola. 2015. Antibody responses to envelope glycoproteins in HIV-1 infection. *Nat. Immunol.* 16: 571–576.
3. Kwong, P. D., J. R. Mascola, and G. J. Nabel. 2013. Broadly neutralizing antibodies and the search for an HIV-1 vaccine: the end of the beginning. *Nat. Rev. Immunol.* 13: 693–701.
4. Klein, F., H. Mouquet, P. Dosenovic, J. F. Scheid, L. Scharf, and M. C. Nussenzweig. 2013. Antibodies in HIV-1 vaccine development and therapy. *Science* 341: 1199–1204.
5. Sanders, R. W., R. Derking, A. Cupo, J. P. Julien, A. Yasmeen, N. de Val, H. J. Kim, C. Blattner, A. T. de la Peña, J. Korzun, et al. 2013. A next-generation cleaved, soluble HIV-1 Env trimer, BG505 SOSIP.664 gp140, expresses multiple epitopes for broadly neutralizing but not non-neutralizing antibodies. *PLoS Pathog.* 9: e1003618.
6. Guenaga, J., N. de Val, K. Tran, Y. Feng, K. Satchwell, A. B. Ward, and R. T. Wyatt. 2015. Well-ordered trimeric HIV-1 subtype B and C soluble spike mimetics generated by negative selection display native-like properties. *PLoS Pathog.* 11: e1004570.
7. Sharma, S. K., N. de Val, S. Bale, J. Guenaga, K. Tran, Y. Feng, V. Dubrovskaya, A. B. Ward, and R. T. Wyatt. 2015. Cleavage-independent HIV-1 Env trimers engineered as soluble native spike mimetics for vaccine design. *Cell Reports* 11: 539–550.

8. Dosenovic, P., L. von Boehmer, A. Escolano, J. Jardine, N. T. Freund, A. D. Gitlin, A. T. McGuire, D. W. Kulp, T. Oliveira, L. Scharf, et al. 2015. Immunization for HIV-1 broadly neutralizing antibodies in Human Ig knockin mice. *Cell* 161: 1505–1515.
9. Jardine, J. G., T. Ota, D. Sok, M. Pauthner, D. W. Kulp, O. Kalyuzhniy, P. D. Skog, T. C. Thinnes, D. Bhullar, B. Briney, et al. 2015. HIV-1 VACCINES. Priming a broadly neutralizing antibody response to HIV-1 using a germline-targeting immunogen. *Science* 349: 156–161.
10. McGuire, A. T., A. M. Dreyer, S. Carbonetti, A. Lippy, J. Glenn, J. F. Scheid, H. Mouquet, and L. Stamatatos. 2014. HIV antibodies. Antigen modification regulates competition of broad and narrow neutralizing HIV antibodies. *Science* 346: 1380–1383.
11. Malherbe, D. C., F. Pissani, D. N. Sather, B. Guo, S. Pandey, W. F. Sutton, A. B. Stuart, H. Robins, B. Park, S. J. Krebs, et al. 2014. Envelope variants circulating as initial neutralization breadth developed in two HIV-infected subjects stimulate multiclade neutralizing antibodies in rabbits. *J. Virol.* 88: 12949–12967.
12. Bricault, C. A., J. M. Kovacs, J. P. Nkolola, K. Yusim, E. E. Giorgi, J. L. Shields, J. Perry, C. L. Lavine, A. Cheung, K. Ellingson-Strouss, et al. 2015. A multivalent clade C HIV-1 Env trimer cocktail elicits a higher magnitude of neutralizing antibodies than any individual component. *J. Virol.* 89: 2507–2519.
13. Rerks-Ngarm, S., P. Pitisuttithum, S. Nitayaphan, J. Kaewkungwal, J. Chiu, R. Paris, N. Premsri, C. Namwat, M. de Souza, E. Adams, et al; MOPH-TAVEG Investigators. 2009. Vaccination with ALVAC and AIDSVAX to prevent HIV-1 infection in Thailand. *N. Engl. J. Med.* 361: 2209–2220.
14. Haynes, B. F., P. B. Gilbert, M. J. McElrath, S. Zolla-Pazner, G. D. Tomaras, S. M. Alam, D. T. Evans, D. C. Montefiori, C. Karnasuta, R. Sutthent, et al. 2012. Immune-correlates analysis of an HIV-1 vaccine efficacy trial. *N. Engl. J. Med.* 366: 1275–1286.
15. Robb, M. L., S. Rerks-Ngarm, S. Nitayaphan, P. Pitisuttithum, J. Kaewkungwal, P. Kunasol, C. Khamboonruang, P. Thongcharoen, P. Morgan, M. Benenson, et al. 2012. Risk behaviour and time as covariates for efficacy of the HIV vaccine regimen ALVAC-HIV (vCP1521) and AIDSVAX B/E: a post-hoc analysis of the Thai phase 3 efficacy trial RV 144. *Lancet Infect. Dis.* 12: 531–537.
16. Yates, N. L., H. X. Liao, Y. Fong, A. deCamp, N. A. Vandergrift, W. T. Williams, S. M. Alam, G. Ferrari, Z. Y. Yang, K. E. Seaton, et al. 2014. Vaccine-induced Env V1-V2 IgG3 correlates with lower HIV-1 infection risk and declines soon after vaccination. *Sci. Transl. Med.* 6: 228ra39.
17. Sundling, C., Z. Zhang, G. E. Phad, Z. Sheng, Y. Wang, J. R. Mascola, Y. Li, R. T. Wyatt, L. Shapiro, and G. B. Karlsson Hedestam. 2014. Single-cell and deep sequencing of IgG-switched macaque B cells reveal a diverse Ig repertoire following immunization. *J. Immunol.* 192: 3637–3644.
18. Sundling, C., Y. Li, N. Huynh, C. Poulsen, R. Wilson, S. O'Dell, Y. Feng, J. R. Mascola, R. T. Wyatt, and G. B. Karlsson Hedestam. 2012. High-resolution definition of vaccine-elicited B cell responses against the HIV primary receptor binding site. *Sci. Transl. Med.* 4: 142ra96.
19. Dai, K., L. He, S. N. Khan, S. O'Dell, K. McKee, K. Tran, Y. Li, C. Sundling, C. D. Morris, J. R. Mascola, et al. 2015. Rhesus Macaque B-Cell Responses to an HIV-1 Trimer Vaccine Revealed by Unbiased Longitudinal Repertoire Analysis. *MBio* 6: e01375–e15.
20. Sundling, C., M. N. Forsell, S. O'Dell, Y. Feng, B. Chakrabarti, S. S. Rao, K. Loré, J. R. Mascola, R. T. Wyatt, I. Douagi, and G. B. Karlsson Hedestam. 2010. Soluble HIV-1 Env trimers in adjuvant elicit potent and diverse functional B cell responses in primates. *J. Exp. Med.* 207: 2003–2017.
21. Wu, X., Z. Y. Yang, Y. Li, C. M. Hogerkorp, W. R. Schief, M. S. Seaman, T. Zhou, S. D. Schmidt, L. Wu, L. Xu, et al. 2010. Rational design of envelope identifies broadly neutralizing human monoclonal antibodies to HIV-1. *Science* 329: 856–861.
22. Sundling, C., G. Phad, I. Douagi, M. Navis, and G. B. Karlsson Hedestam. 2012. Isolation of antibody V(D)J sequences from single cell sorted rhesus macaque B cells. *J. Immunol. Methods* 386: 85–93.
23. Tiller, T., E. Meffre, S. Yurasov, M. Tsuiji, M. C. Nussenzweig, and H. Wardemann. 2008. Efficient generation of monoclonal antibodies from single human B cells by single cell RT-PCR and expression vector cloning. *J. Immunol. Methods* 329: 112–124.
24. Wardemann, H., S. Yurasov, A. Schaefer, J. W. Young, E. Meffre, and M. C. Nussenzweig. 2003. Predominant autoantibody production by early human B cell precursors. *Science* 301: 1374–1377.
25. Alamyar, E., V. Giudicelli, S. Li, P. Duroux, and M. P. Lefranc. 2012. IMGT/HighV-QUEST: the IMGT(R) web portal for immunoglobulin (IG) or antibody and T cell receptor (TR) analysis from NGS high throughput and deep sequencing. *Immunome Res.* DOI: 10.4172/1745-7580.1000056.
26. Ye, J., N. Ma, T. L. Madden, and J. M. Ostell. 2013. IgBLAST: an immunoglobulin variable domain sequence analysis tool. *Nucleic Acids Res.* 41: W34–W40.
27. Altschul, S. F., T. L. Madden, A. A. Schäffer, J. Zhang, Z. Zhang, W. Miller, and D. J. Lipman. 1997. Gapped BLAST and PSI-BLAST: a new generation of protein database search programs. *Nucleic Acids Res.* 25: 3389–3402.
28. Wu, X., T. Zhou, J. Zhu, B. Zhang, I. Georgiev, C. Wang, X. Chen, N. S. Longo, M. Louder, K. McKee, et al; NISC Comparative Sequencing Program. 2011. Focused evolution of HIV-1 neutralizing antibodies revealed by structures and deep sequencing. *Science* 333: 1593–1602.
29. Larkin, M. A., G. Blackshields, N. P. Brown, R. Chenna, P. A. McGettigan, H. McWilliam, F. Valentin, I. M. Wallace, A. Wilm, R. Lopez, et al. 2007. Clustal W and Clustal X version 2.0. *Bioinformatics* 23: 2947–2948.
30. Li, M., F. Gao, J. R. Mascola, L. Stamatatos, V. R. Polonis, M. Koutsoukos, G. Voss, P. Goepfert, P. Gilbert, K. M. Greene, et al. 2005. Human immunodeficiency virus type 1 env clones from acute and early subtype B infections for standardized assessments of vaccine-elicited neutralizing antibodies. *J. Virol.* 79: 10108–10125.
31. Seaman, M. S., H. Janes, N. Hawkins, L. E. Grandpre, C. Devoy, A. Giri, R. T. Coffey, L. Harris, B. Wood, M. G. Daniels, et al. 2010. Tiered categorization of a diverse panel of HIV-1 Env pseudoviruses for assessment of neutralizing antibodies. *J. Virol.* 84: 1439–1452.
32. Wu, X., T. Zhou, S. O'Dell, R. T. Wyatt, P. D. Kwong, and J. R. Mascola. 2009. Mechanism of human immunodeficiency virus type 1 resistance to monoclonal antibody B12 that effectively targets the site of CD4 attachment. *J. Virol.* 83: 10892–10907.
33. Pantophlet, R., E. Ollmann Saphire, P. Poignard, P. W. Parren, I. A. Wilson, and D. R. Burton. 2003. Fine mapping of the interaction of neutralizing and non-neutralizing monoclonal antibodies with the CD4 binding site of human immunodeficiency virus type 1 gp120. *J. Virol.* 77: 642–658.
34. Zhou, T., L. Xu, B. Dey, A. J. Hessell, D. Van Ryk, S. H. Xiang, X. Yang, M. Y. Zhang, M. B. Zwick, J. Arthos, et al. 2007. Structural definition of a conserved neutralization epitope on HIV-1 gp120. *Nature* 445: 732–737.
35. Saphire, E. O., P. W. Parren, R. Pantophlet, M. B. Zwick, G. M. Morris, P. M. Rudd, R. A. Dwek, R. L. Stanfield, D. R. Burton, and I. A. Wilson. 2001. Crystal structure of a neutralizing human IGG against HIV-1: a template for vaccine design. *Science* 293: 1155–1159.
36. Breden, F., C. Lepik, N. S. Longo, M. Montero, P. E. Lipsky, and J. K. Scott. 2011. Comparison of antibody repertoires produced by HIV-1 infection, other chronic and acute infections, and systemic autoimmune disease. *PLoS One* 6: e16857.
37. Zhou, T., R. M. Lynch, L. Chen, P. Acharya, X. Wu, N. A. Doria-Rose, M. G. Joyce, D. Lingwood, C. Soto, R. T. Bailer, et al; NISC Comparative Sequencing Program. 2015. Structural Repertoire of HIV-1-Neutralizing Antibodies Targeting the CD4 Supersite in 14 Donors. *Cell* 161: 1280–1292.
38. Kwong, P. D., R. Wyatt, J. Robinson, R. W. Sweet, J. Sodroski, and W. A. Hendrickson. 1998. Structure of an HIV gp120 envelope glycoprotein in complex with the CD4 receptor and a neutralizing human antibody. *Nature* 393: 648–659.
39. Chen, L., Y. D. Kwon, T. Zhou, X. Wu, S. O'Dell, L. Cavacini, A. J. Hessell, M. Pancera, M. Tang, L. Xu, et al. 2009. Structural basis of immune evasion at the site of CD4 attachment on HIV-1 gp120. *Science* 326: 1123–1127.
40. Poulsen, T. R., A. Jensen, J. S. Haurum, and P. S. Andersen. 2011. Limits for antibody affinity maturation and repertoire diversification in hypervaccinated humans. *J. Immunol.* 187: 4229–4235.
41. Davis, M. M., and Chien, Y.H. 1999. *T Cell Antigen Receptors*. Lippincott-Raven, Philidelphia.
42. Moody, M. A., N. L. Yates, J. D. Amos, M. S. Drinker, J. A. Eudailey, T. C. Gurley, D. J. Marshall, J. F. Whitesides, X. Chen, A. Foulger, et al. 2012. HIV-1 gp120 vaccine induces affinity maturation in both new and persistent antibody clonal lineages. *J. Virol.* 86: 7496–7507.
43. Choi, Y. W., A. Herman, D. DiGiusto, T. Wade, P. Marrack, and J. Kappler. 1990. Residues of the variable region of the T-cell-receptor beta-chain that interact with *S. aureus* toxin superantigens. *Nature* 346: 471–473.
44. Garcia, K. C., M. Degano, R. L. Stanfield, A. Brunmark, M. R. Jackson, P. A. Peterson, L. Teyton, and I. A. Wilson. 1996. An alphabeta T cell receptor structure at 2.5 A and its orientation in the TCR-MHC complex. *Science* 274: 209–219.
45. Li, H., A. Llera, and R. A. Mariuzza. 1998. Structure-function studies of T-cell receptor-superantigen interactions. *Immunol. Rev.* 163: 177–186.
46. Potter, K. N., Y. Li, and J. D. Capra. 1996. Staphylococcal protein A simultaneously interacts with framework region 1, complementarity-determining region 2, and framework region 3 on human VH3-encoded Igs. *J. Immunol.* 157: 2982–2988.
47. Throsby, M., E. van den Brink, M. Jongeneelen, L. L. Poon, P. Alard, L. Cornelissen, A. Bakker, F. Cox, E. van Deventer, Y. Guan, et al. 2008. Heterosubtypic neutralizing monoclonal antibodies cross-protective against H5N1 and H1N1 recovered from human IgM+ memory B cells. *PLoS One* 3: e3942.
48. Ekiert, D. C., G. Bhabha, M. A. Elsliger, R. H. Friesen, M. Jongeneelen, M. Throsby, J. Goudsmit, and I. A. Wilson. 2009. Antibody recognition of a highly conserved influenza virus epitope. *Science* 324: 246–251.
49. Li, Y., S. O'Dell, L. M. Walker, X. Wu, J. Guenaga, Y. Feng, S. D. Schmidt, K. McKee, M. K. Louder, J. E. Ledgerwood, et al. 2011. Mechanism of neutralization by the broadly neutralizing HIV-1 monoclonal antibody VRC01. *J. Virol.* 85: 8954–8967.
50. Wang, Y., P. Kapoor, R. Parks, A. Silva-Sanchez, S. M. Alam, L. Verkoczy, H. X. Liao, Y. Zhuang, P. Burrows, M. Levinson, et al. 2016. HIV-1 gp140 epitope recognition is influenced by immunoglobulin DH gene segment sequence. *Immunogenetics* 68: 145–155.
51. Tran, K., C. Poulsen, J. Guenaga, N. de Val, R. Wilson, C. Sundling, Y. Li, R. L. Stanfield, I. A. Wilson, A. B. Ward, et al. 2014. Vaccine-elicited primate antibodies use a distinct approach to the HIV-1 primary receptor binding site informing vaccine redesign. [Published erratum appears in 2014 *Proc Natl Acad Sci U S A.* 111: E1159.] *Proc. Natl. Acad. Sci. USA* 111: E738–E747.
52. Sanders, R. W., M. J. van Gils, R. Derking, D. Sok, T. J. Ketas, J. A. Burger, G. Ozorowski, A. Cupo, C. Simonich, L. Goo, et al. 2015. HIV-1 VACCINES. HIV-1 neutralizing antibodies induced by native-like envelope trimers. *Science* 349: aac4223.
53. Klein, F., R. Diskin, J. F. Scheid, C. Gaebler, H. Mouquet, I. S. Georgiev, M. Pancera, T. Zhou, R. B. Incesu, B. Z. Fu, et al. 2013. Somatic mutations of the immunoglobulin framework are generally required for broad and potent HIV-1 neutralization. *Cell* 153: 126–138.